

NASA TECHNICAL NOTE



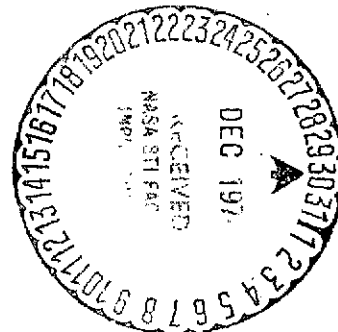
NASA TN D-7827

NASA TN D-7827

(NASA-TN-D-7827)	SUBSONIC ROLL-DAMPING	N75-12938
	CHARACTERISTICS OF A SERIES OF WINGS	
(NASA)	39 p HC \$3.75	CSCL 01B
		Unclas
		H1/05 05102

# SUBSONIC ROLL-DAMPING CHARACTERISTICS OF A SERIES OF WINGS

by *Richmond P. Boyden*  
*Langley Research Center*  
*Hampton, Va. 23665*



1. Report No. NASA TN D-7827	2. Government Accession No.	3. Recipient's Catalog No.	
4. Title and Subtitle SUBSONIC ROLL-DAMPING CHARACTERISTICS OF A SERIES OF WINGS		5. Report Date December 1974	6. Performing Organization Code
		8. Performing Organization Report No. L-8854	
7. Author(s) Richmond P. Boyden		10. Work Unit No. 754-62-01-06	11. Contract or Grant No.
9. Performing Organization Name and Address NASA Langley Research Center Hampton, Va. 23665		13. Type of Report and Period Covered Technical Note	
		14. Sponsoring Agency Code	
12. Sponsoring Agency Name and Address National Aeronautics and Space Administration Washington, D.C. 20546		15. Supplementary Notes	
16. Abstract The aerodynamic damping in roll of a series of wings has been investigated in the Langley high-speed 7- by 10-foot tunnel at Mach numbers ranging from 0.2 to 0.8 by use of a forced oscillatory-roll technique. Tests were conducted on wings of aspect ratio 6 with sweep angles of 25°, 35°, and 45° and on 35° swept wings of aspect ratios 4 and 5.			
17. Key Words (Suggested by Author(s)) Dynamic stability Roll damping Aerodynamics		18. Distribution Statement Unclassified -- Unlimited  STAR Category 01	
19. Security Classif. (of this report) Unclassified	20. Security Classif. (of this page) Unclassified	21. No. of Pages 37	22. Price* \$3.75

# SUBSONIC ROLL-DAMPING CHARACTERISTICS OF A SERIES OF WINGS

By Richmond P. Boyden  
Langley Research Center

## SUMMARY

The aerodynamic damping in roll of a series of wings has been investigated in the Langley high-speed 7- by 10-foot tunnel at Mach numbers ranging from 0.2 to 0.8 by use of a forced oscillatory-roll technique. Tests were conducted on wings of aspect ratio 6 with sweep angles of  $25^\circ$ ,  $35^\circ$ , and  $45^\circ$  and on  $35^\circ$  swept wings of aspect ratios 4 and 5. The wings with the higher sweep were found to maintain favorable values of the roll damping over a wider range of angles of attack. The deflection of a leading-edge flap resulted in improved roll damping at the higher angles of attack. Comparisons have been made with theoretical estimates of the roll damping at  $0^\circ$  angle of attack over the Mach number range, but the comparisons showed only fair agreement.

## INTRODUCTION

The subsonic and transonic aerodynamics of wings operating well out of the range of potential flow and into the separated-flow regime is a subject of continuing interest because of the direct applicability of the study to highly maneuverable aircraft and to aircraft operating near the stall. Both the performance and the response of the aircraft can be adversely affected by the consequences of separated flow on the lifting surfaces. In addition, the aerodynamic characteristics of lifting surfaces, such as the damping in roll, are difficult to predict for nonpotential flow.

The objective of this study was to make an assessment of the effect of several wing design parameters on the aerodynamic damping in roll in regions of separated flow. The wing parameters that were varied during this investigation were the wing sweep, the aspect ratio, the airfoil section, and the deflection of the leading- and trailing-edge flaps. The range of Mach numbers was from 0.20 to 0.80 and the maximum angle of attack reached was nearly  $22^\circ$ .

This investigation is a continuation of previous work done at Langley Research Center on the roll damping of wings using various methods. Some of this work is listed as references 1 to 9. Among the methods used in these references to obtain roll-damping characteristics are free rolling, forced steady roll, forced oscillatory roll, twisted wings, rolling flow, and free flight. The present study used the forced oscillatory-roll technique.

The experimental results for an angle of attack of  $0^\circ$  are compared with a potential-flow theory over the range of Mach numbers from 0.2 to 0.8.

### SYMBOLS

The aerodynamic parameters in this paper are referred to the body system of axes. In figure 1, the rolling-moment coefficient, the angles, and the angular velocity are shown in the positive sense. The axes originate at the assumed center of oscillation which was located 66.80 cm (26.30 in.) rearward of the model nose and 0.318 cm (0.125 in.) below the fuselage axis of symmetry.

Units of measurement are presented in the International System of Units (SI) with U.S. Customary Units given parenthetically. Details on the use of SI, together with the physical constants and conversion factors, are given in reference 10. A dot over a quantity indicates a first derivative with respect to time.

A.R. aspect ratio

b reference span, centimeters (inches)

$C_l$  rolling-moment coefficient,  $\frac{\text{Rolling moment}}{q_\infty S b}$

$$C_{l_p} = \frac{\partial C_l}{\partial \left( \frac{p b}{2V} \right)} \text{ per radian}$$

$C_{l_p} + C_{l_{\dot{\beta}}} \sin \alpha$  damping-in-roll parameter, per radian

$$C_{l_{\dot{p}}} = \frac{\partial C_l}{\partial \left( \frac{\dot{p} b^2}{4V^2} \right)} \text{ per radian}$$

$$C_{l_\beta} = \frac{\partial C_l}{\partial \beta} \text{ per radian}$$

$C_{l_\beta} \sin \alpha - k^2 C_{l_{\dot{p}}}$  rolling moment due to roll displacement parameter, per radian

$$C_{l\dot{\beta}} = \frac{\partial C_l}{\partial \left( \frac{\dot{\beta} b}{2V} \right)} \text{ per radian}$$

$\bar{c}$	mean geometric chord, centimeters (inches)
$c_r$	root chord, centimeters (inches)
$f$	frequency of oscillation, hertz
$k$	reduced-frequency parameter, $\frac{\omega b}{2V}$ , radians
$M$	free-stream Mach number
$p$	angular velocity of model about X-axis, radians/second
$q_\infty$	free-stream dynamic pressure, pascals (pounds/foot <sup>2</sup> )
$S$	reference area, meters <sup>2</sup> (feet <sup>2</sup> )
$V$	free-stream velocity, meters/second (feet/second)
$X, Y, Z$	body system of axes
$\alpha$	angle of attack, degrees
$\beta$	angle of sideslip, degrees
$\Lambda$	sweep angle of wing quarter-chord line, degrees
$\lambda$	taper ratio
$\omega$	angular velocity, $2\pi f$ , radians/second

## APPARATUS

### Models

Six wing models were studied which incorporated variations in wing sweep, in aspect ratio, and in the position of maximum thickness. One of these wings had provision

for testing with leading- and trailing-edge flaps. The flush brackets supporting the leading and trailing edges in the undeflected case were removed and were replaced with brackets having a built-in deflection about the 20-percent-chord line and the 70-percent-chord line, respectively. Both the leading- and trailing-edge flaps extended from 0.1375b/2 to the wing tip. Except for the leading- and trailing-edge flaps, each wing was machined from a solid steel panel. The wings were attached to a steel wing adapter which formed a section of the center fuselage and served to carry the wing loads through to the strain-gage balance. The fuselage forebody and the rear fuselage section were of fiberglass construction. These wing-body models were originally used in a study of buffet onset in reference 11, and the wing designation numbers used in reference 11 have been retained. (See table I.) The only change in the models used previously has been the use of a 5.08-cm (2.00-in.) shorter rear fuselage section. The basic model dimensions are shown in figure 2(a) and in tables I and II. Sketches of the different wing planforms are shown in figure 2(b). The photographs in figure 3 show one of the wing-fuselage models mounted in the test section of the high-speed 7- by 10-foot tunnel on the forced-oscillation roll mechanism.

#### Forced-Oscillation Mechanism

A sketch of the small amplitude oscillatory-roll mechanism used for this investigation is shown in figure 4. The basic principles of operation of the oscillatory-roll mechanism are the same as those for the small amplitude rigidly forced-oscillation system of reference 12. A two horsepower electric motor with an eccentric drive oscillates the sting and the model in an essentially sinusoidal motion. The model is rigidly forced in a fixed  $2.5^\circ$  amplitude oscillation about the sting axis (body X-axis) at a variable frequency. A mechanical torsion spring internal to the sting is attached to the front of the strain-gage balance section. This attachment permits the model to be oscillated at the frequency for velocity resonance whereby the mechanical torsion spring, plus any aerodynamic spring, balances out the model inertia. The only torque then required to oscillate the model at that particular frequency is equal to the torque caused by the aerodynamic damping. (See ref. 12.)

Although the models may be oscillated at frequencies from about 1 to 30 hertz, the damping torque is obtained most accurately by operating at velocity resonance. The rolling-moment strain gages are located forward of all the bearings and the other friction-producing devices. A strain-gage bridge is mounted on the mechanical torsion spring to provide a signal proportional to the model angular displacement in roll.

#### Wind Tunnel

The facility used for this investigation was the Langley high-speed 7- by 10-foot tunnel. This single-return, atmospheric, continuous-flow facility had a closed test sec-

tion during this series of tests and was capable of Mach numbers from the low subsonic to in excess of 0.90. Additional information on the tunnel and on its operating conditions is contained in reference 13. The sting-support system, when used with the forced-oscillation roll mechanism (figs. 3 and 4), provided an angle-of-attack range from about  $-4^\circ$  to  $22^\circ$ .

## MEASUREMENTS AND REDUCTION OF DATA

Measurements were made of the amplitude of the torque required to oscillate the model in roll  $T_X$ , of the amplitude of the angular displacement in roll of the model with respect to the fixed portion of the sting  $\Phi$ , of the phase angle  $\sigma$  between  $T_X$  and  $\Phi$ , and of the angular velocity of the forced oscillation  $\omega$ . The viscous-damping moment coefficient in roll  $C_X$ , for this single-degree-of-freedom system, was computed as

$$C_X = \frac{T_X \sin \sigma}{\omega \Phi} \quad (1)$$

The spring-inertia parameter in roll was computed as

$$K_X - I_X \omega^2 = \frac{T_X \cos \sigma}{\Phi} \quad (2)$$

where  $K_X$  is the torsional spring coefficient of the system and  $I_X$  is the moment of inertia of the system about the body X-axis.

For this investigation, the damping-in-roll parameter was computed as

$$C_{l_p} + C_{l_{\dot{\beta}}} \sin \alpha = - \frac{2V}{q_\infty S b^2} \left[ (C_X)_{\text{wind on}} - (C_X)_{\text{wind off}} \right] \quad (3)$$

and the rolling moment due to roll displacement parameter as

$$C_{l_\beta} \sin \alpha - k^2 C_{l_p} = - \frac{1}{q_\infty S b} \left[ (K_X - I_X \omega^2)_{\text{wind on}} - (K_X - I_X \omega^2)_{\text{wind off}} \right] \quad (4)$$

The wind-off value of  $C_X$  is determined at the frequency of wind-off velocity resonance, where the mechanical spring balances the model inertia. However, the value of  $C_X$  is independent of frequency and can be determined most accurately at the frequency of velocity resonance. The wind-on and wind-off values of  $K_X - I_X \omega^2$  are determined at the same frequency since  $K_X - I_X \omega^2$  is a function of frequency.

## TESTS

The dynamic stability parameters were measured at Mach numbers of 0.20, 0.40, 0.60, and 0.80 over an angle-of-attack range which varied depending on the specific con-

figuration. All the models were tested over the entire available range of angles of attack from about  $-4^\circ$  to  $22^\circ$  at Mach numbers of 0.20 and 0.40. For the Mach numbers of 0.60 and 0.80, however, the upper limit on the angle of attack was restricted to a range between  $4^\circ$  and  $12^\circ$  by an unwanted vibration of the model-sting combination in the pitch plane and by the balance load limits. Nominal test conditions are listed in the following table:

Mach number	Dynamic pressure		Reynolds number	
	Pa	lb/ft <sup>2</sup>	per m	per ft
0.20	2 869	59.9	$4.30 \times 10^6$	$1.31 \times 10^6$
.40	10 192	212.9	8.05	2.45
.60	20 072	419.2	10.75	3.28
.80	29 794	622.3	12.32	3.76

The amplitude of the roll oscillation for this investigation was about  $2.5^\circ$  and was determined by the mechanical throw of the actuating crank. The range of the reduced-frequency parameter was from 0.034 to 0.208.

The effective increment in the angle of attack at the wing tip induced by the oscillatory-roll rate may be determined by multiplying the amplitude of the roll oscillation by the reduced-frequency parameter. For these wings, the increment in the angle of attack at the wing tip ranged from approximately  $0.085^\circ$  to  $0.52^\circ$ .

The wind-off frequency for velocity resonance of this series of wing-body models ranged from 2.39 to 2.59 hertz. Since this range of oscillation frequency was considered to be too low for consistent wind-on data, all the models were tested at a constant wind-on frequency of oscillation of about 4.0 hertz, with the exception of wing 2. It was run at about 5.0 hertz for  $M = 0.20$  and  $M = 0.40$ ; the frequency was then lowered to 4.0 hertz for the remainder of the tests.

In order to insure a turbulent boundary layer over the model, carborundum grains were applied as three-dimensional roughness to the model nose and to the leading edge of the wing. The grit size and location chosen were those used on the same models in reference 11. These specifications consisted of transition strips of No. 150 carborundum grit, 1.27 cm (0.50 in.) behind the leading edge of the wings on the upper and lower surfaces and 2.54 cm (1.00 in.) behind the fuselage nose as described in reference 14.

## RESULTS AND DISCUSSION

The results are presented in figures 5 to 8. The damping-in-roll parameter  $C_{l_p} + C_{l_{\dot{\beta}}} \sin \alpha$  and the rolling moment due to roll displacement parameter  $C_{l_{\beta}} \sin \alpha - k^2 C_{l_p}$ , are plotted against the angle of attack.

## Effect of Wing Sweep

The first set of results shows the effect of various wing sweep angles of  $25^\circ$ ,  $35^\circ$ , and  $45^\circ$  on a wing with an aspect ratio of 6 for Mach numbers of 0.20, 0.40, 0.60, and 0.80. These results are shown in figures 5(a) to 5(d). The roll damping for wing 1 ( $\Lambda = 25^\circ$ ) falls off rapidly with an increasing angle of attack above  $6^\circ$  at Mach numbers of 0.20 and 0.40 and above  $4^\circ$  at Mach numbers of 0.60 and 0.80. At  $M = 0.20$  the damping for wing 1 decreased to less than 20 percent of its  $0^\circ$  angle-of-attack magnitude; while, for  $M = 0.40$  and  $M = 0.60$ , the roll damping decreased to approximately zero damping at about  $10^\circ$  and  $8^\circ$ , respectively. This decrease in the roll damping with an increased angle of attack is primarily a result of tip stall or separation on the outboard sections of the wing as noted in references 6 and 8. At higher angles of attack, the damping in roll tends to increase with  $\alpha$  for Mach numbers of 0.20 and 0.40 with the higher sweep wings having the more negative values of  $C_{l_p} + C_{l_{\dot{\beta}}} \sin \alpha$ . The angle of attack at Mach numbers of 0.60 and 0.80 had to be restricted because of the allowable balance loads and the unwanted model-sting vibrations in the pitch plane.

Generally, there is a decrease in the level of the roll damping at  $\alpha = 0^\circ$  with an increase in wing sweep from  $25^\circ$  to  $45^\circ$ . The exception to this was at  $M = 0.20$  and  $M = 0.40$  where the  $25^\circ$  and  $35^\circ$  swept wings did not follow this trend. Increasing the wing sweep also had the effect of decreasing the amount of dropoff in the roll damping at the higher angles of attack. For wing 3 ( $\Lambda = 45^\circ$ ), there was an apparent peak in the damping-in-roll parameter at  $\alpha = 6^\circ$  for  $M = 0.20$  and  $M = 0.40$  which was somewhat larger than the  $\alpha = 0^\circ$  value.

The rolling moment due to roll displacement parameter  $C_{l_{\dot{\beta}}} \sin \alpha - k^2 C_{l_p}$  is included with the damping-in-roll parameter in figures 5 to 8 for completeness since both components of the rolling moment are measured simultaneously. The usefulness of this parameter is greatly reduced, however, because of the  $\sin \alpha$  multiplier in the  $C_{l_{\dot{\beta}}}$  term. The parameter does serve to indicate gross effects such as a sign change in the dihedral effect. The actual contribution of the  $C_{l_p}$  term is considered to be small inasmuch as tests at different frequencies (or values of  $k$ ) usually show a negligible frequency effect.

## Effect of Aspect Ratio

The effect on the damping in roll of various aspect ratios in the range of 4, 5, and 6 for a wing with  $35^\circ$  wing sweep is shown in figures 6(a) to 6(d). Increasing the aspect ratio increases the damping in roll in the low angle-of-attack range.

## Effect of Leading-Edge and Trailing-Edge Flaps

The results for a  $35^\circ$  swept wing of aspect ratio 6, with and without leading- and trailing-edge flaps, are shown in figures 7(a) to 7(d). This particular wing model (wing 6) had a NACA 64A008 airfoil section, while the remainder of the wings utilized in this investigation had a NACA 63A008 airfoil section as shown in table I. With the leading-edge flap deflected  $30^\circ$ , the roll damping is less than that for the basic wing for angles of attack less than  $2^\circ$  for Mach numbers of 0.60 and below. However, the roll damping does not fall off until  $\alpha$  is greater than  $12^\circ$  for Mach numbers of 0.20 and 0.40 and until  $\alpha$  is greater than  $8^\circ$  for the Mach number of 0.60. Because the roll damping does not fall off, the leading-edge flap would appear to have a favorable effect on the damping in roll for Mach numbers less than 0.80. At  $M = 0.80$ , the roll damping for the deflected leading-edge case is much lower than that for the basic wing over the somewhat limited range of angle of attack.

The  $12^\circ$  deflection of the trailing edge generally caused the roll damping to fall off much sooner with the angle of attack than did the basic wing. Consequently, it showed little possibility of being a method of improving the trend of roll damping with angle of attack.

## Effect of Position of Maximum Thickness

Figure 8 is a comparison of the roll-damping results with a variation in the position of maximum thickness of the airfoil sections from 0.3 chord to 0.4 chord for an aspect-ratio-6 wing with  $30^\circ$  sweep. At a Mach number of 0.20, there is a clear difference in the level of the damping-in-roll parameter for the two airfoil sections. The wing with the more forward position of maximum thickness, the NACA 63A008 section, has the higher roll damping. At the other Mach numbers this difference was less apparent, except for isolated data points such as at  $M = 0.40$  and a  $14^\circ$  angle of attack.

## Comparison of Theoretical Estimates and Experimental Results

Theoretical estimates of the damping-in-roll derivative  $C_{l_p}$  were computed for both the sweep series and the aspect-ratio series of wings. The method used was the modified Multhopp lifting-surface theory of reference 15. These theoretical estimates give the potential flow result for a zero-thickness planform, and they have been compared with averaged experimental data for an angle of attack of about  $0^\circ$  as shown in figure 9. The experimental results are for the damping-in-roll parameter  $C_{l_p} + C_{l_\beta} \sin \alpha$ , but for  $\alpha = 0^\circ$  the contribution of the second term would be zero.

For the wing-sweep series in figure 9(a), the experimental results show a more positive damping than did the theoretical estimates. The experimental variation with

Mach number for the three wings is only in fair agreement with that predicted by the method of reference 15. Also, the theoretical trend of decreased roll damping with increased wing sweep was not realized experimentally at  $M = 0.20$  and  $M = 0.40$ .

One reason that the experimental results have more damping in roll than the predicted values is because the wing is located a vertical distance  $z$  along the Z-axis above the actual roll axis. This vertical separation results in an increment to the predicted roll damping  $\Delta C_{lp}$ , which is primarily a function of the wing dihedral effect  $\Delta C_{lp} \approx \frac{2z}{b} C_{l\beta}$ . Estimates of this increment for this series of wings give  $\Delta C_{lp} \approx -0.01$  to  $-0.02$ , a condition which can account for only a portion of the differences seen in figure 9(a).

The comparison of the experimental results with the theoretical estimates for the aspect-ratio series of wings is shown in figure 9(b). As in the previous figure, the experimental data show the higher values of roll damping over the Mach number range. The theoretical variation of increased roll damping with increased aspect ratio was verified by the experimental results.

### SUMMARY OF RESULTS

The results from an experimental investigation into the roll-damping characteristics of a series of wings at subsonic speeds using a forced oscillatory-roll technique are as follows:

1. For the wing series of aspect ratio 6, a  $45^\circ$  wing sweep resulted in more favorable values of the damping-in-roll parameter at angles of attack in excess of  $6^\circ$  than did wing sweeps of  $25^\circ$  and  $35^\circ$ .
2. The deflection of a leading-edge flap on a wing of aspect ratio 6 with  $35^\circ$  sweep had a favorable effect for Mach numbers less than 0.80 by extending to a higher angle of attack the point at which the roll damping began to decrease.
3. The effect of the position of maximum thickness on the roll damping was not conclusive and only showed a clear difference at a Mach number of 0.20.
4. A comparison of the experimental results for an angle of attack of  $0^\circ$  and the theoretical estimates showed only fair agreement.

Langley Research Center,  
National Aeronautics and Space Administration,  
Hampton, Va., November 5, 1974.

## REFERENCES

1. Kuhn, Richard E.; and Myers, Boyd C., II: Effects of Mach Number and Sweep on the Damping-in-Roll Characteristics of Wings of Aspect Ratio 4. NACA RM L9E10, 1949.
2. Letko, William; and Wolhart, Walter D.: Effect of Sweepback on the Low-Speed Static and Rolling Stability Derivatives of Thin Tapered Wings of Aspect Ratio 4. NACA RM L9F14, 1949.
3. Lockwood, Vernard E.: Effects of Sweep on the Damping-in-Roll Characteristics of Three Sweptback Wings Having an Aspect Ratio of 4 at Transonic Speeds. NACA RM L50J19, 1950.
4. Sanders, E. Claude, Jr.: Damping in Roll of Straight and 45° Swept Wings of Various Taper Ratios Determined at High Subsonic, Transonic, and Supersonic Speeds With Rocket-Powered Models. NACA RM L51H14, 1951.
5. Kuhn, Richard E.: Notes on Damping in Roll and Load Distributions in Roll at High Angles of Attack and High Subsonic Speed. NACA RM L53G13a, 1953.
6. Wiggins, James W.; and Kuhn, Richard E.: Wind-Tunnel Investigation of the Effects of Steady Rolling on the Aerodynamic Loading Characteristics of a 45° Sweptback Wing at High Subsonic Speeds. NACA RM L53J01a, 1953.
7. Kuhn, Richard E.; and Wiggins, James W.: Wind-Tunnel Investigation To Determine the Aerodynamic Characteristics in Steady Roll of a Model at High Subsonic Speeds. NACA RM L52K24, 1953.
8. Wiggins, James W.: Wind-Tunnel Investigation of Effect of Sweep on Rolling Derivatives at Angles of Attack up to 13° and at High Subsonic Mach Numbers, Including a Semiempirical Method of Estimating the Rolling Derivatives. NACA TN 4185, 1958. (Supersedes NACA RM L54C26.)
9. Shanks, Robert E.: Low-Subsonic Measurements of Static and Dynamic Stability Derivatives of Six Flat-Plate Wings Having Leading-Edge Sweep Angles of 70° to 84°. NASA TN D-1822, 1963.
10. Mechtly, E. A.: The International System of Units - Physical Constants and Conversion Factors (Second Revision). NASA SP-7012, 1973.
11. Ray, Edward J.; and Taylor, Robert T.: Buffet and Static Aerodynamic Characteristics of a Systematic Series of Wings Determined From a Subsonic Wind-Tunnel Study. NASA TN D-5805, 1970.

12. Braslow, Albert L.; Wiley, Harleth G.; and Lee, Cullen Q.: A Rigidly Forced Oscillation System for Measuring Dynamic-Stability Parameters in Transonic and Supersonic Wind Tunnels. NASA TN D-1231, 1962.
13. Schaefer, William T., Jr.: Characteristics of Major Active Wind Tunnels at the Langley Research Center. NASA TM X-1130, 1965.
14. Braslow, Albert L.; Hicks, Raymond M.; and Harris, Roy V., Jr.: Use of Grit-Type Boundary-Layer-Transition Trips on Wind-Tunnel Models. NASA TN D-3579, 1966.
15. Lamar, John E.: A Modified Multhopp Approach for Predicting Lifting Pressures and Camber Shape for Composite Planforms in Subsonic Flow. NASA TN D-4427, 1968.

TABLE I. - WING CHARACTERISTICS

Wing	Airfoil section	$\Lambda$ , deg	Aspect ratio	$\lambda$	$c_r$		$\bar{c}$		b		S		Fuselage station of leading edge of $c_r$	
					cm	in.	cm	in.	cm	in.	m <sup>2</sup>	ft <sup>2</sup>	cm	in.
1	NACA 63A008	25	6	0.4	21.8	8.57	16.2	6.38	91.4	36.00	0.139	1.50	48.95	19.27
2	NACA 63A008	35	6	.4	21.8	8.57	16.2	6.38	91.4	36.00	0.139	1.50	47.93	18.87
3	NACA 63A008	45	6	.4	21.8	8.57	16.2	6.38	91.4	36.00	0.139	1.50	46.58	18.34
6	NACA 64A008	35	6	.4	21.8	8.57	16.2	6.38	91.4	36.00	0.139	1.50	47.93	18.87
10	NACA 63A008	35	4	.4	26.7	10.50	19.8	7.80	74.7	29.39	0.139	1.50	47.75	18.80
11	NACA 63A008	35	5	.4	23.9	9.39	17.7	6.98	83.5	32.86	0.139	1.50	47.85	18.84

TABLE II. - FUSELAGE ORDINATES

Fuselage station		Radius	
cm	in.	cm	in.
0.00	0.00	0.00	0.00
4.14	1.63	3.71	1.46
6.68	2.63	4.22	1.66
9.22	3.63	4.62	1.82
11.76	4.63	4.95	1.95
14.30	5.63	5.23	2.06
16.84	6.63	5.54	2.18
19.38	7.63	5.74	2.26
21.92	8.63	5.97	2.35
24.46	9.63	6.12	2.41
27.00	10.63	6.22	2.45
98.55	38.80	6.22	2.45
101.09	39.80	6.12	2.41
103.63	40.80	5.99	2.36
106.17	41.80	5.84	2.30
108.71	42.80	5.64	2.22
111.25	43.80	5.44	2.14
113.79	44.80	5.18	2.04
116.33	45.80	4.88	1.92
118.87	46.80	4.57	1.80

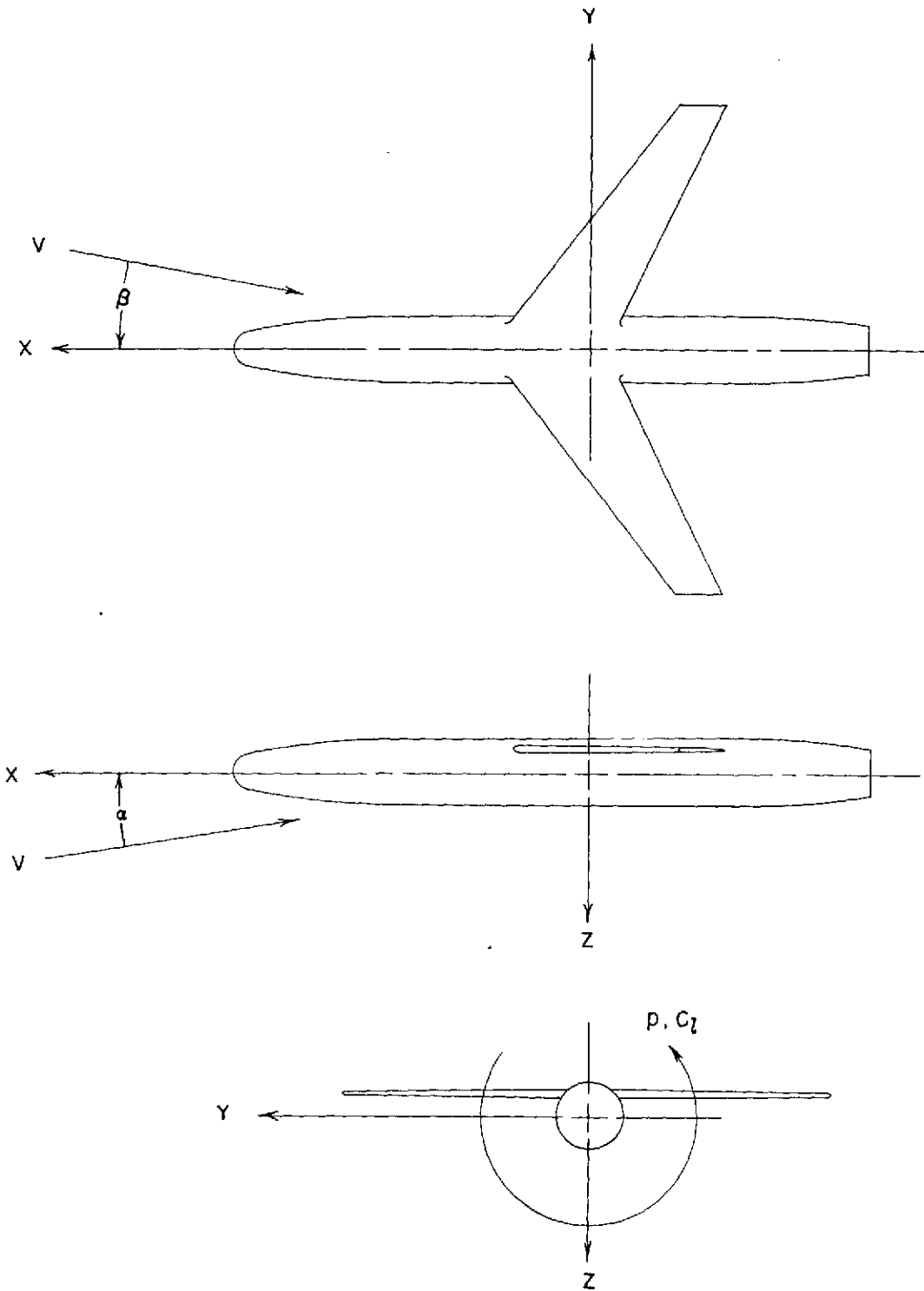
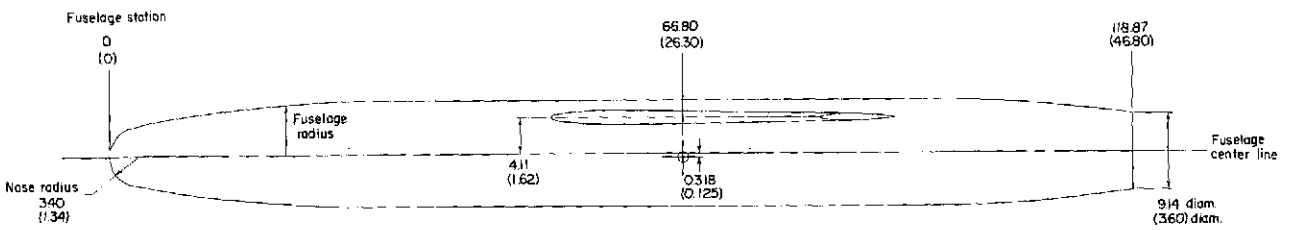
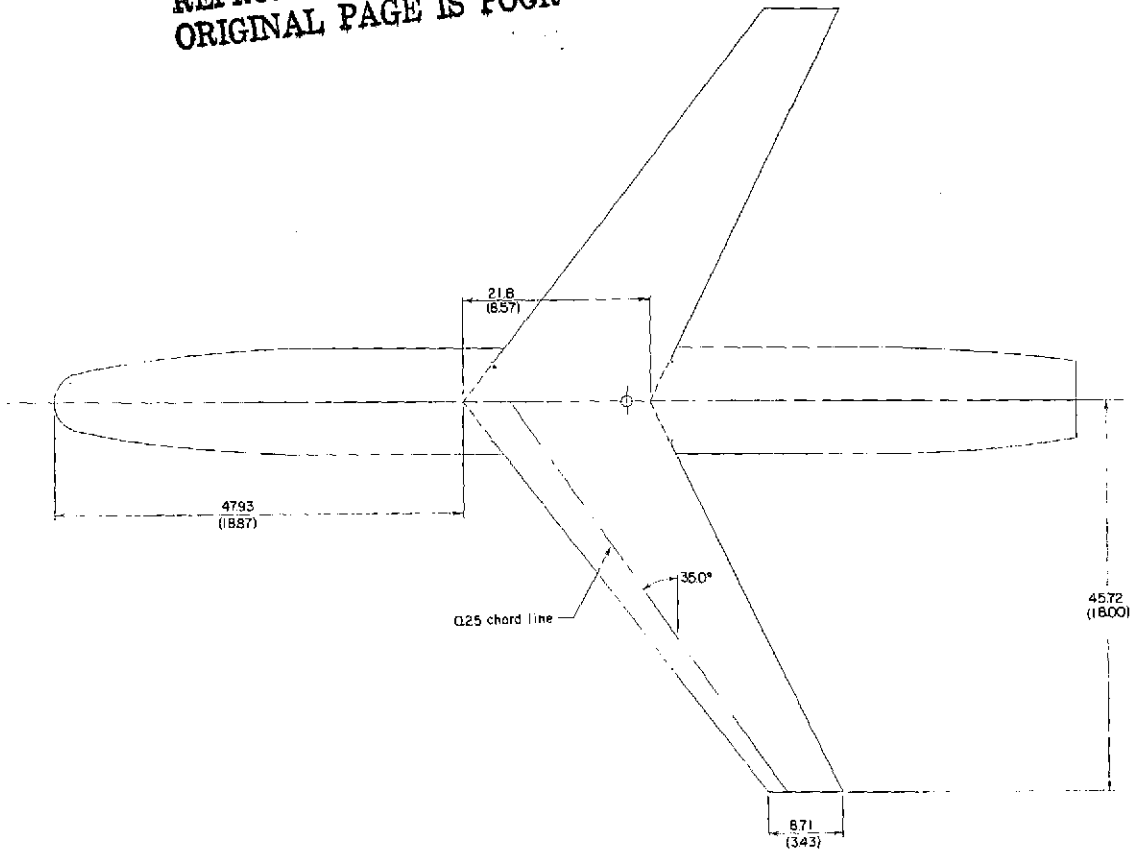


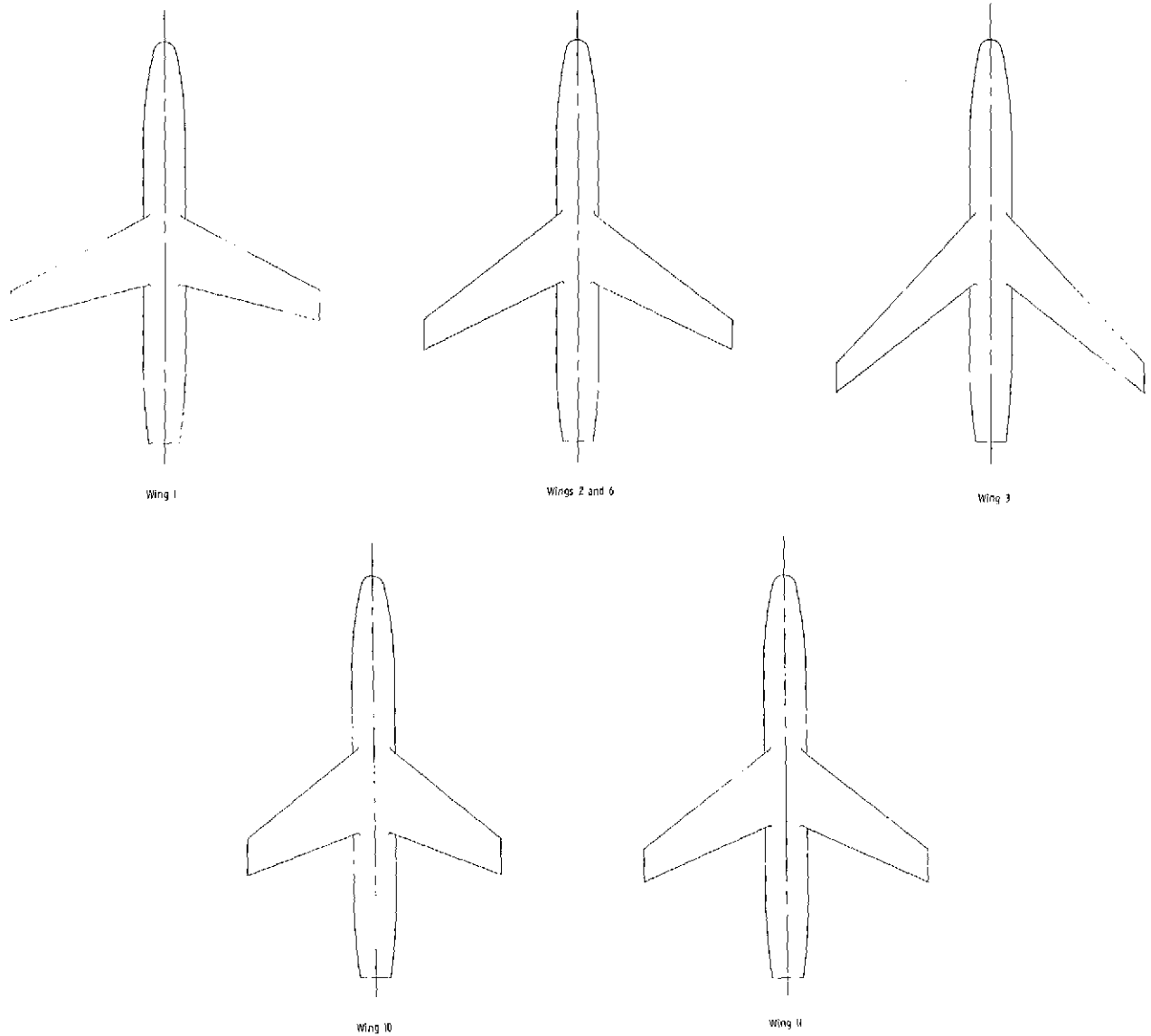
Figure 1.- Body system of axes with the angles, angular velocity, and the rolling-moment coefficient shown in the positive sense.

REPRODUCIBILITY OF THE ORIGINAL PAGE IS POOR



(a) Wing-body model with wing 2 shown.

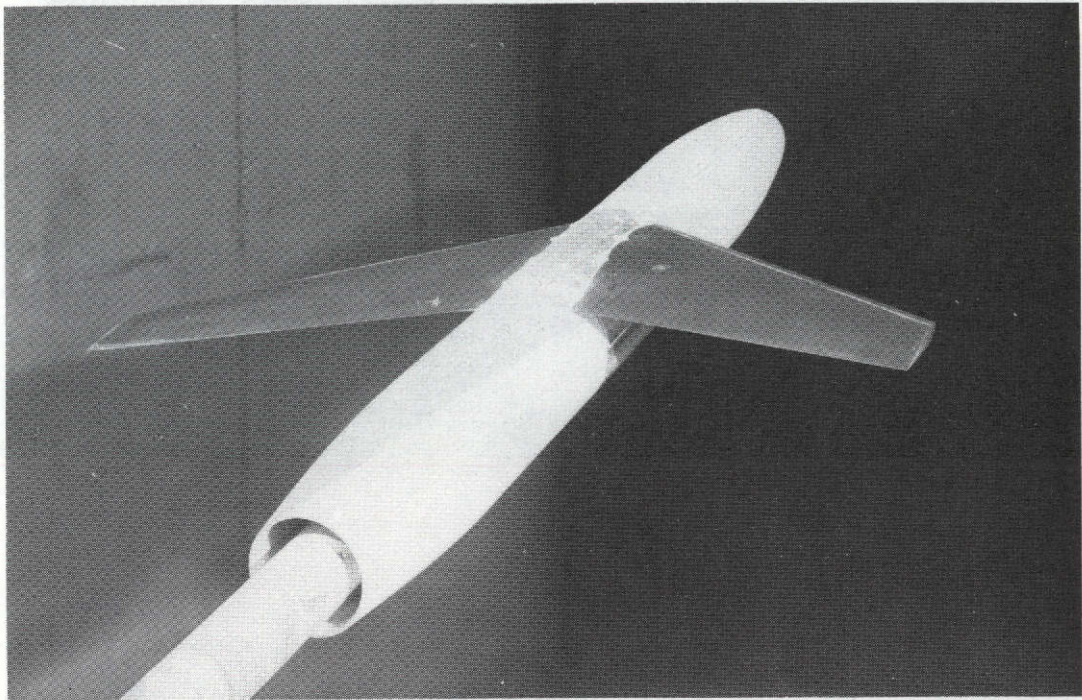
Figure 2.- General arrangement of models. All linear dimensions are in centimeters and parenthetically in inches.



(b) Sketch of the wing-body planforms.

Figure 2.- Concluded.

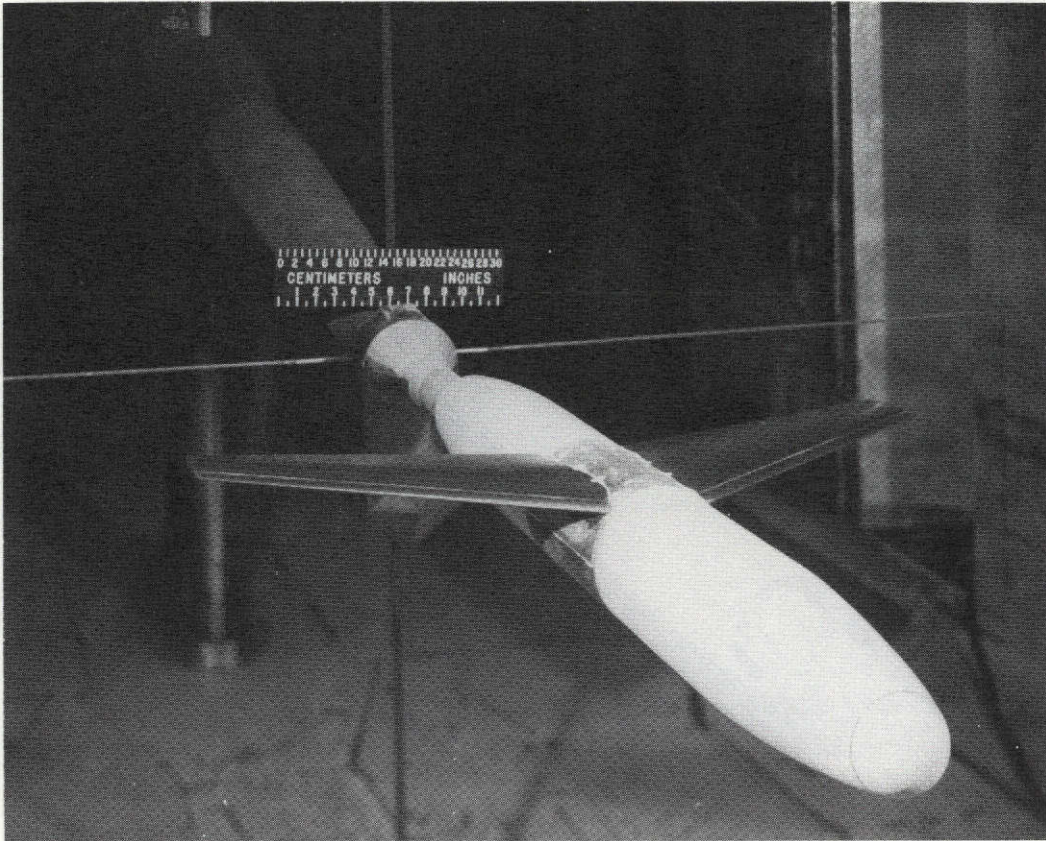
REPRODUCIBILITY OF THE  
ORIGINAL PAGE IS POOR



L-69-6646

(a) Upstream view.

Figure 3.- Wing-body mounted on forced-oscillation roll mechanism in Langley high-speed 7- by 10-foot tunnel.



(b) Downstream view.

L-69-6647

Figure 3.- Concluded.

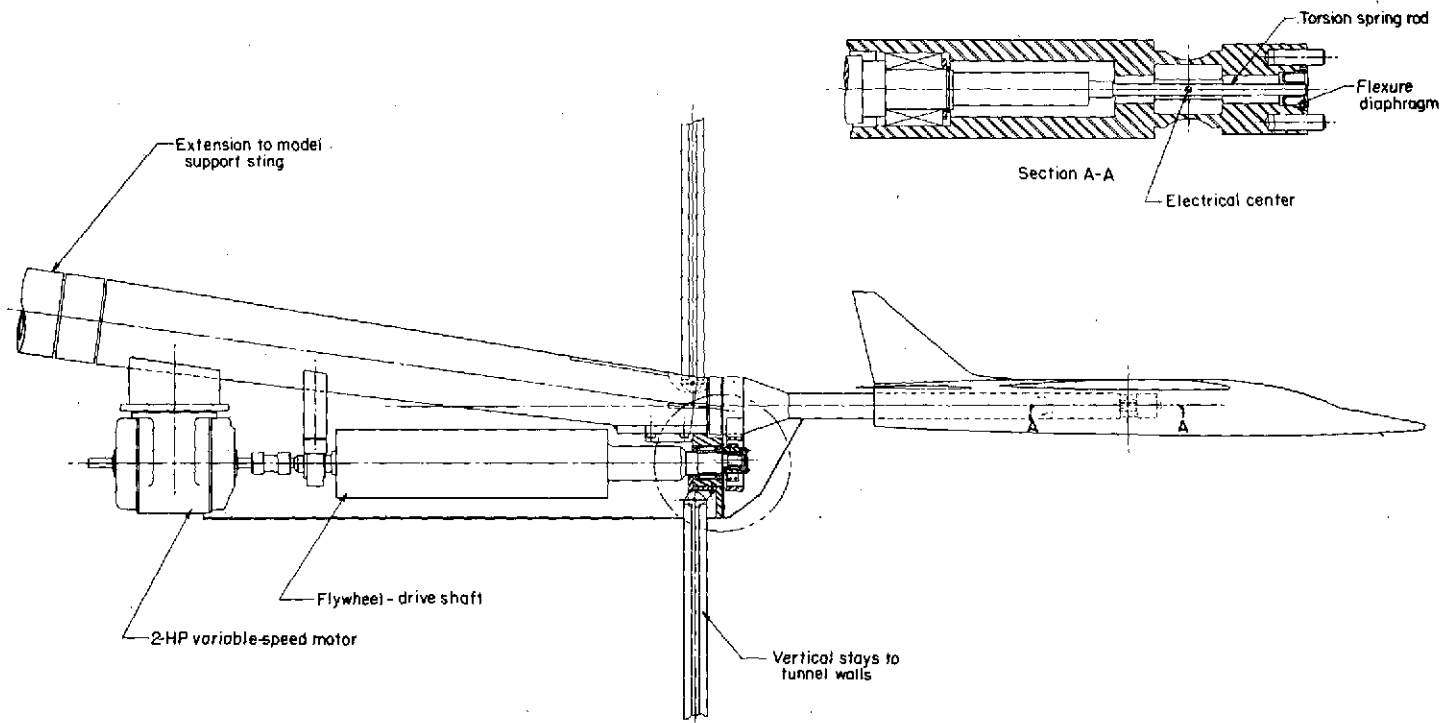
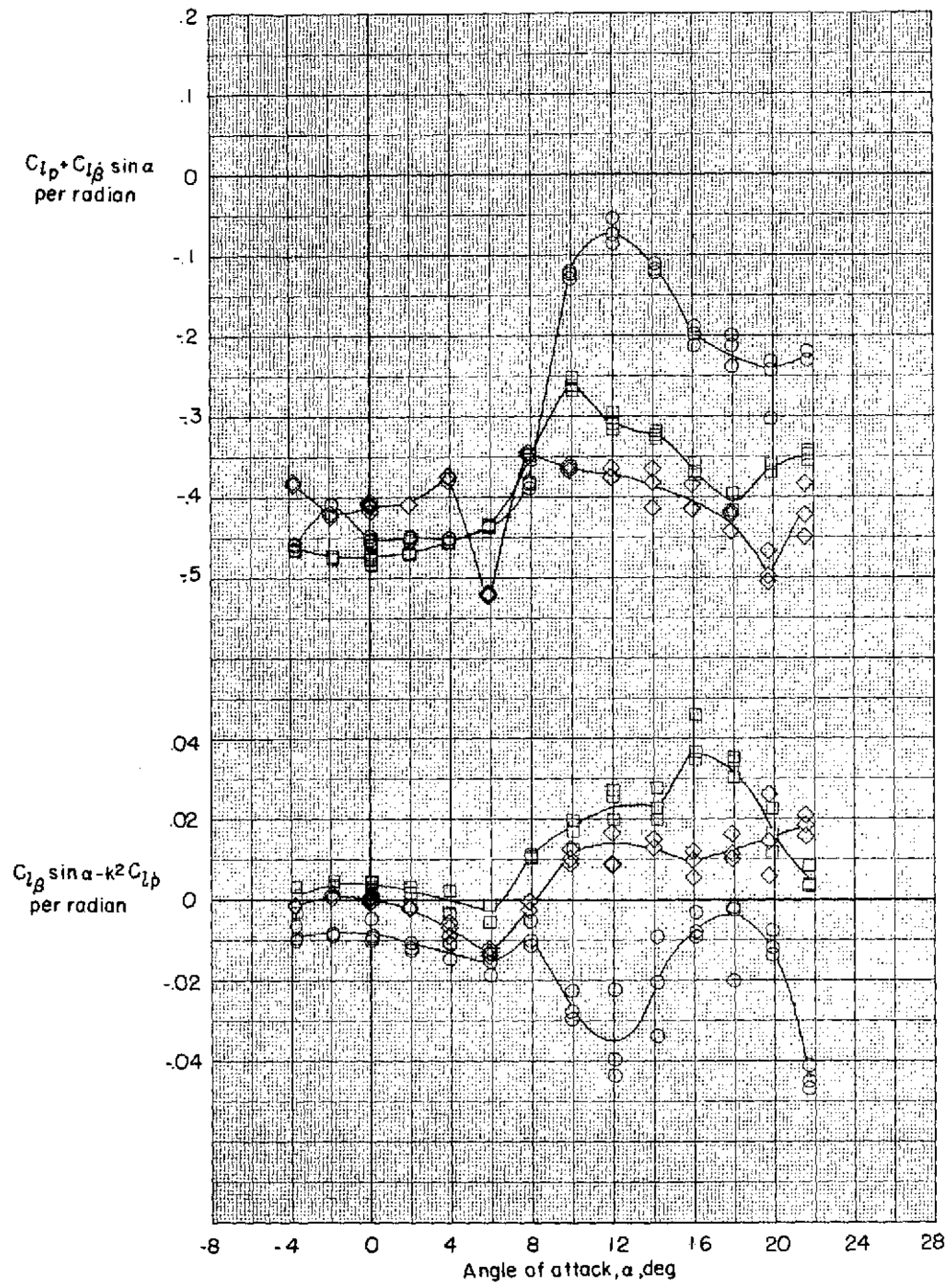


Figure 4. - Forced-oscillation roll mechanism.

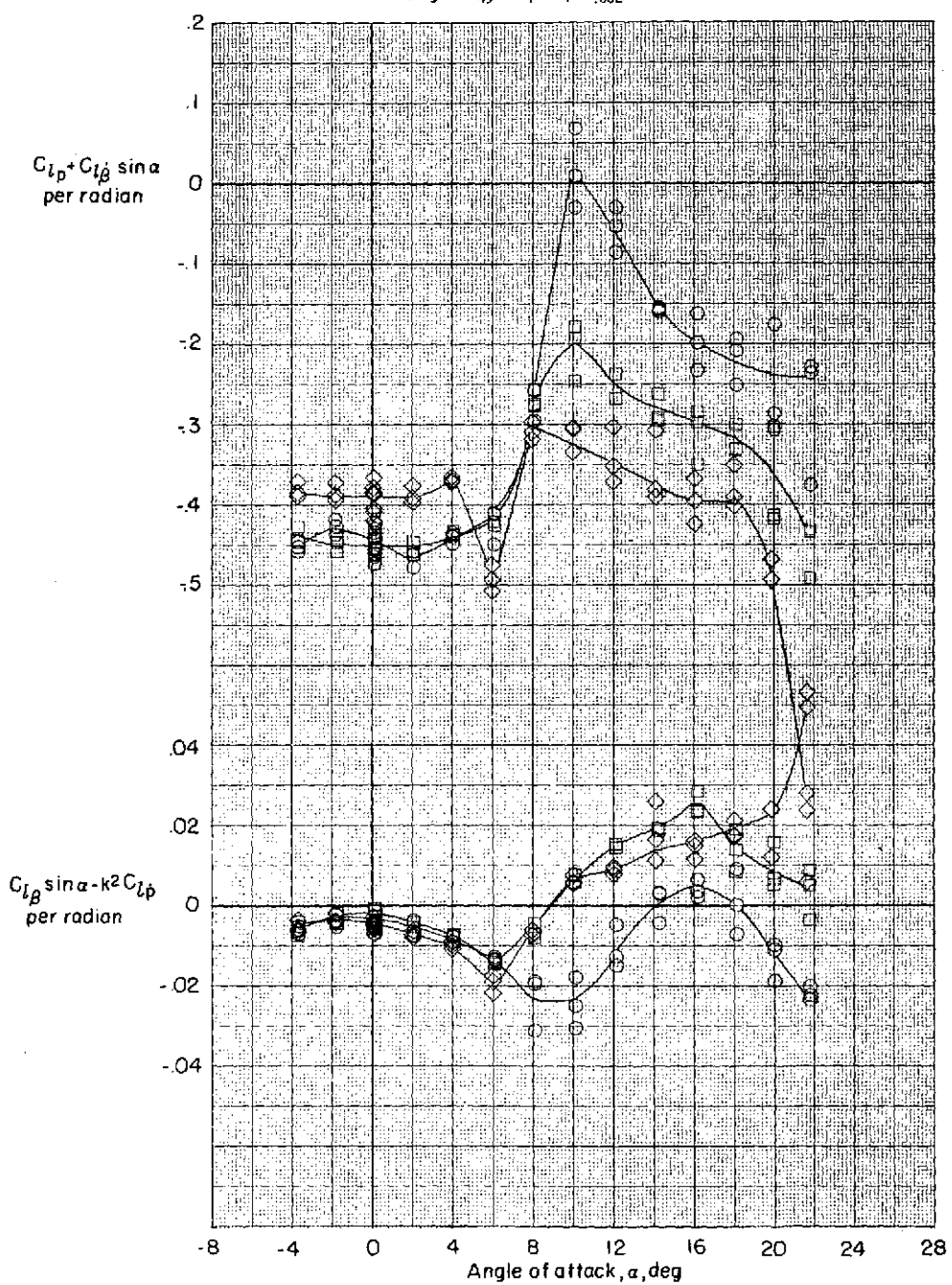
Wing	$\Lambda$	A.R.	M	k
○ 1	25°	6	0.20	0.167
□ 2	35°	↓	↓	.208
◇ 3	45°	↓	↓	.164



(a)  $M = 0.20$ .

Figure 5. - Oscillatory damping in roll and rolling moment due to roll displacement characteristics of a series of wings with sweeps of 25°, 35°, and 45°.

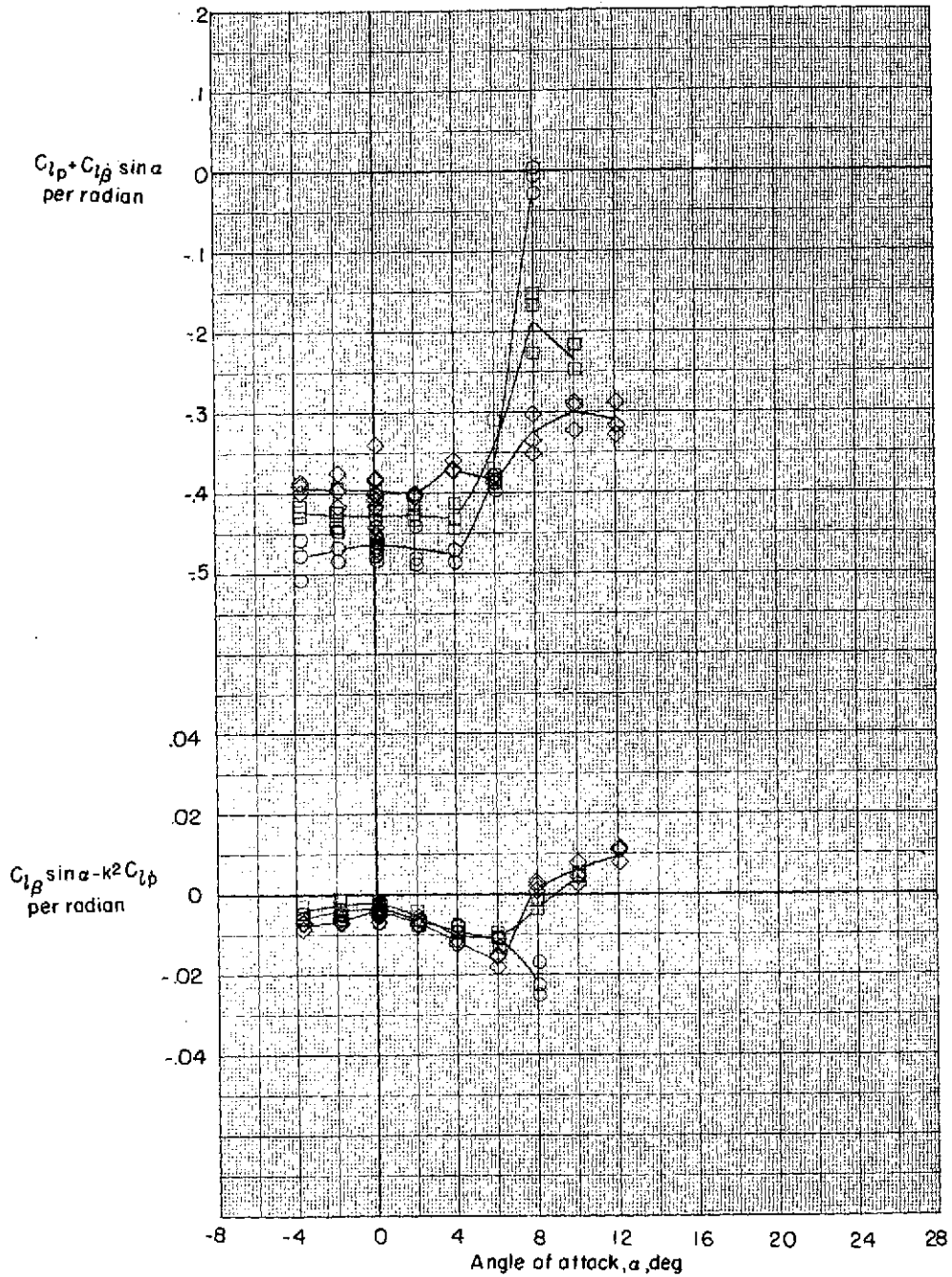
Wing	$\Lambda$	A.R.	M	k
○ 1	25°	6	0.40	0.084
□ 2	35°	↓	↓	.104
◇ 3	45°	↓	↓	.082



(b)  $M = 0.40$ .

Figure 5.- Continued.

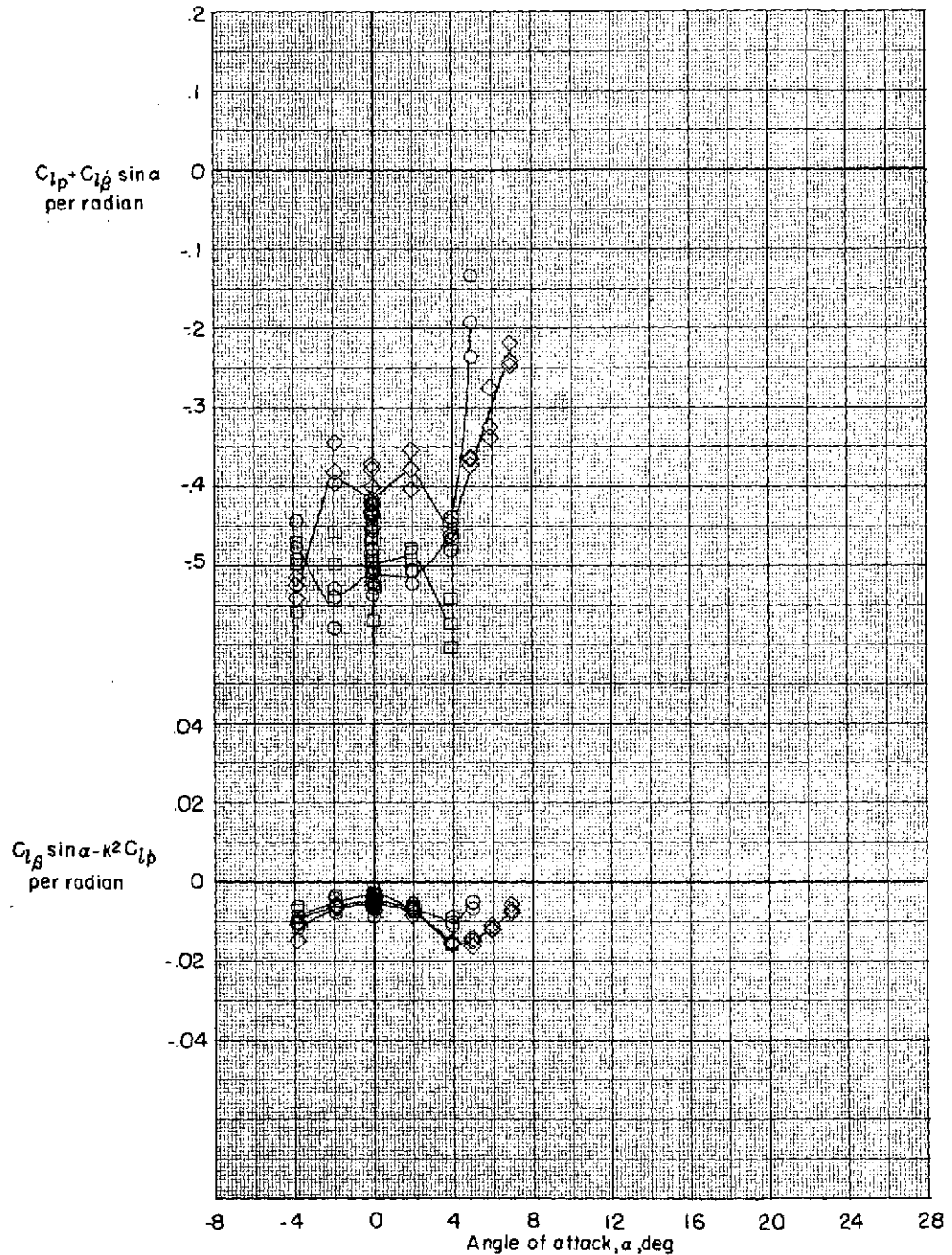
Wing	A	A.R.	M	k
○ 1	25°	6	0.60	0.056
□ 2	35°	↓	↓	.055
◇ 3	45°	↓	↓	.055



(c)  $M = 0.60$ .

Figure 5.- Continued.

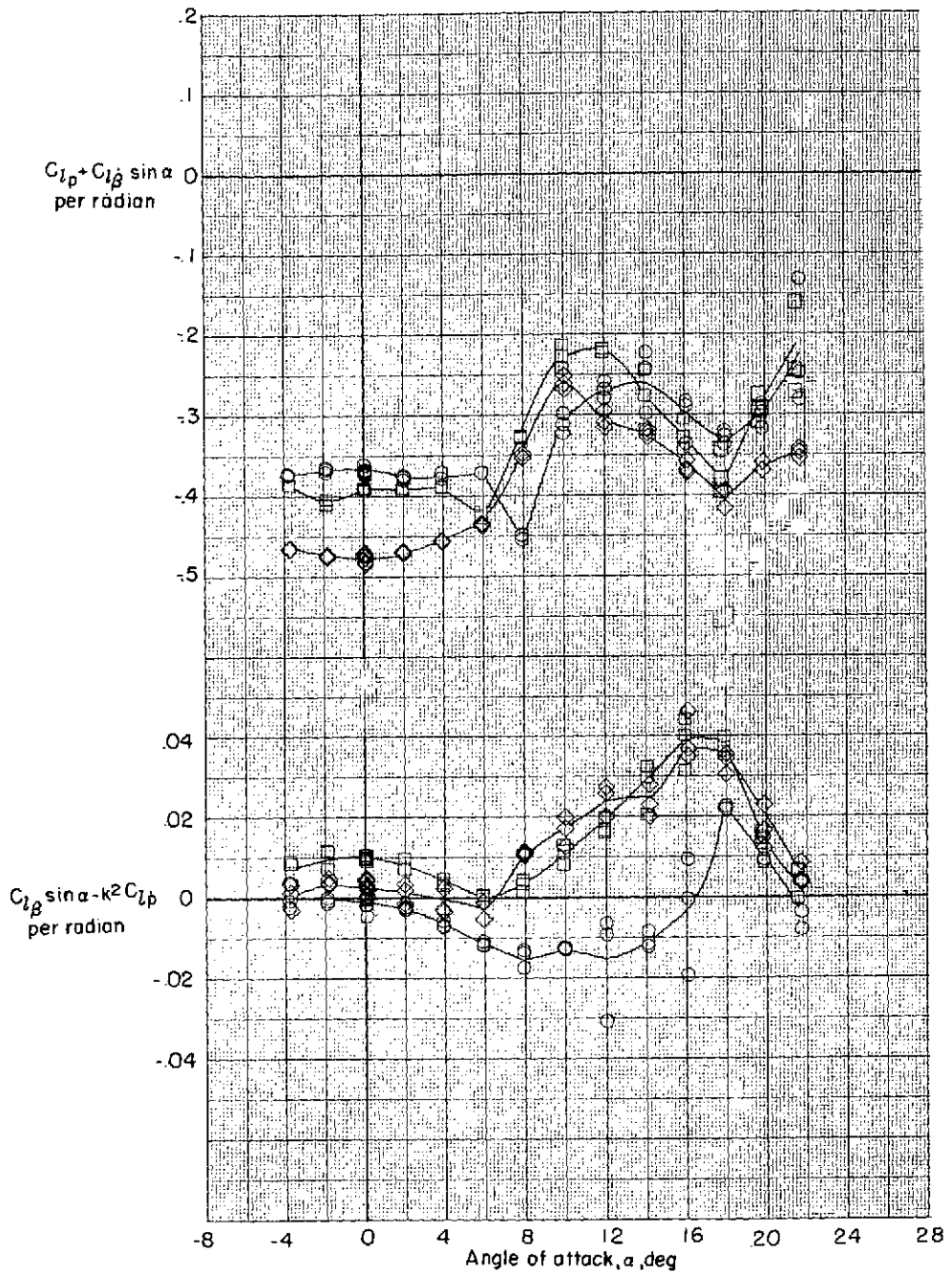
Wing	$\Lambda$	A.R.	M	k
○ 1	25°	6	0.80	0.042
□ 2	35°	↓	↓	↓
◇ 3	45°	↓	↓	↓



(d)  $M = 0.80$ .

Figure 5.- Concluded.

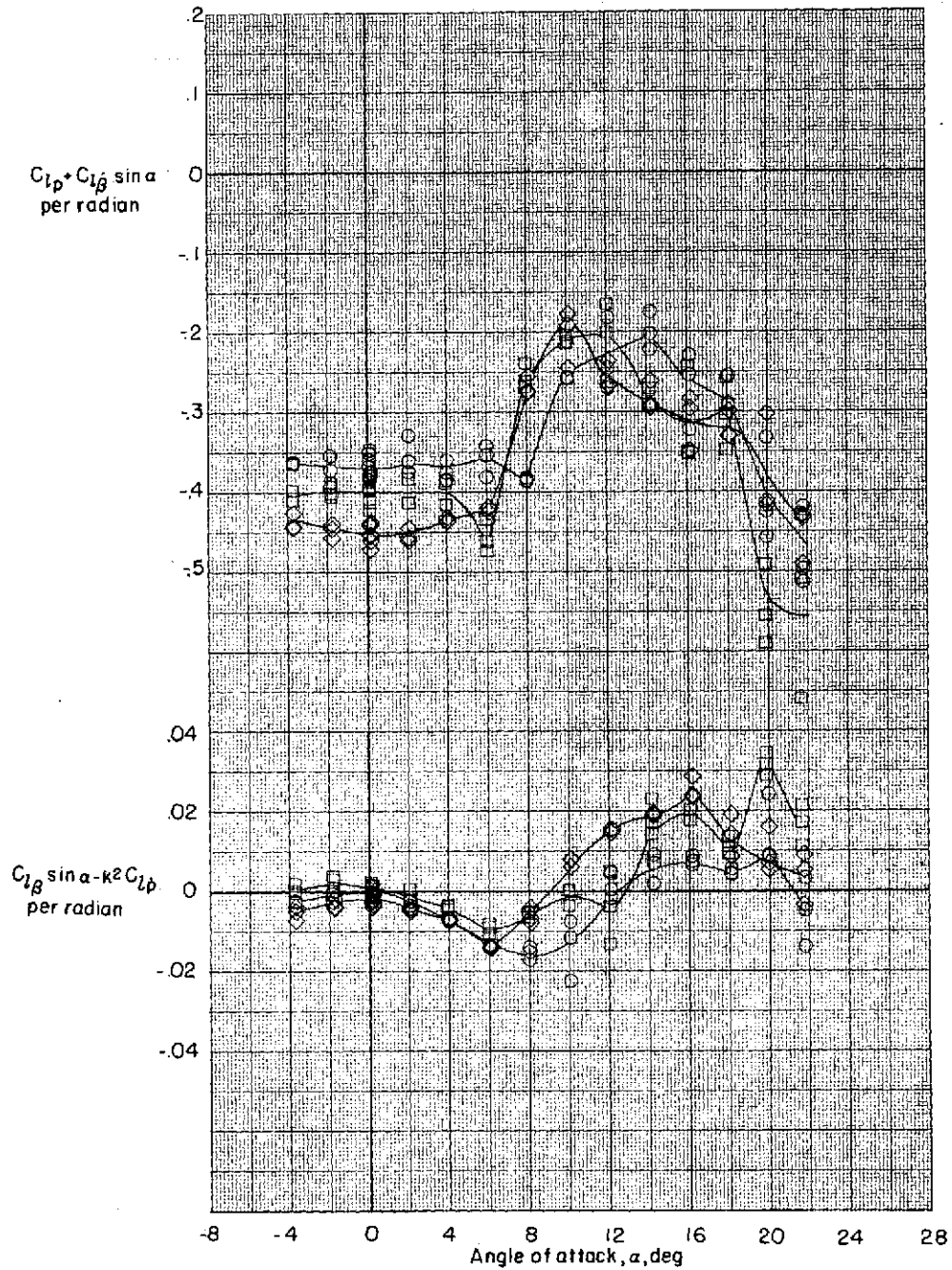
Wing	A	A.R.	M	k	
○	10	35°	4	0.20	0.135
□	11	↓	5	↓	.149
◇	2	↓	6	↓	.208



(a)  $M = 0.20$ .

Figure 6.- Oscillatory damping in roll and rolling moment due to roll displacement characteristics of a series of wings of aspect ratio 4, 5, and 6.

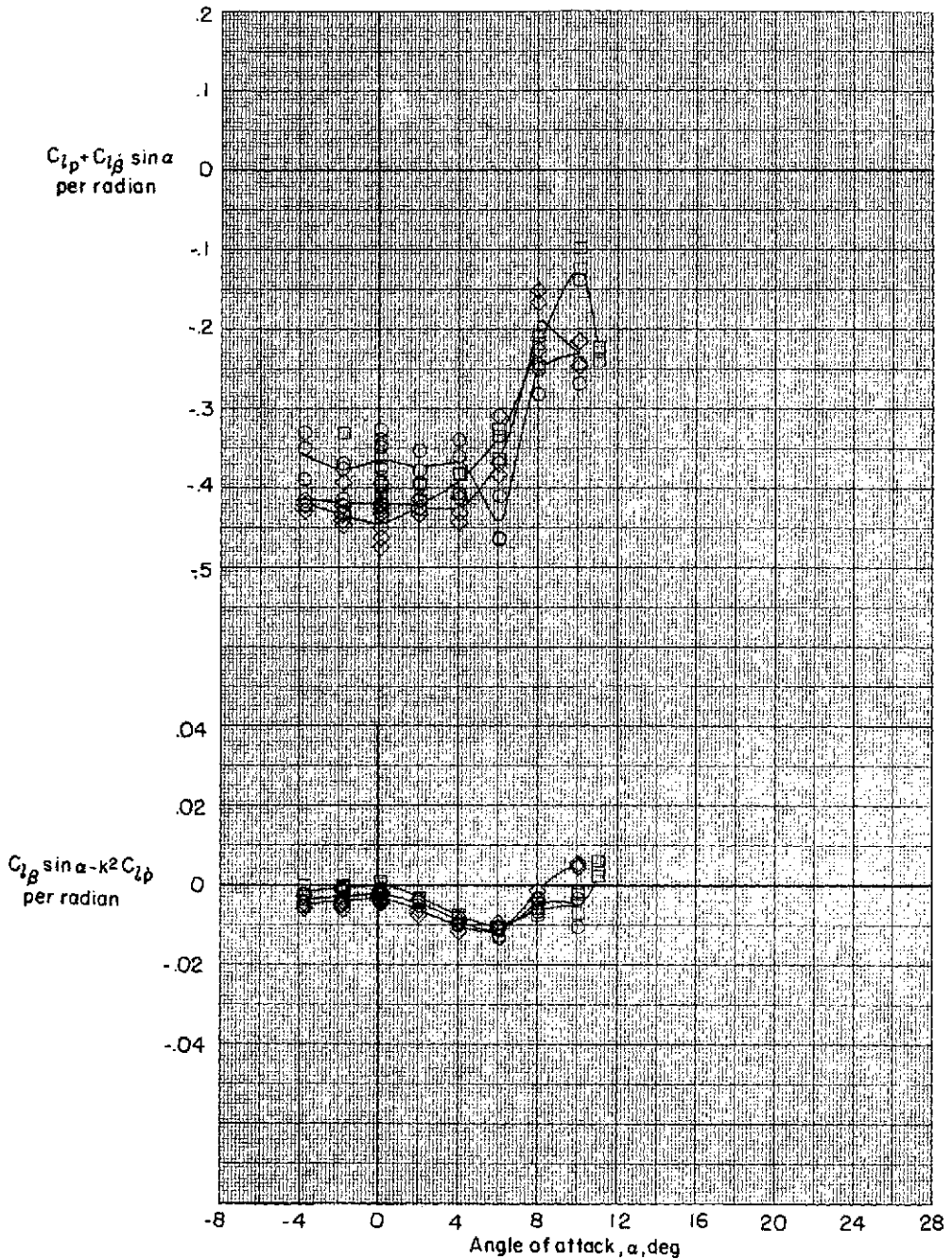
Wing	$\Lambda$	A.R.	M	k
○	10	35°	4	0.40
□	11	↓	5	.075
◇	2	↓	6	.104



(b)  $M = 0.40$ .

Figure 6.- Continued.

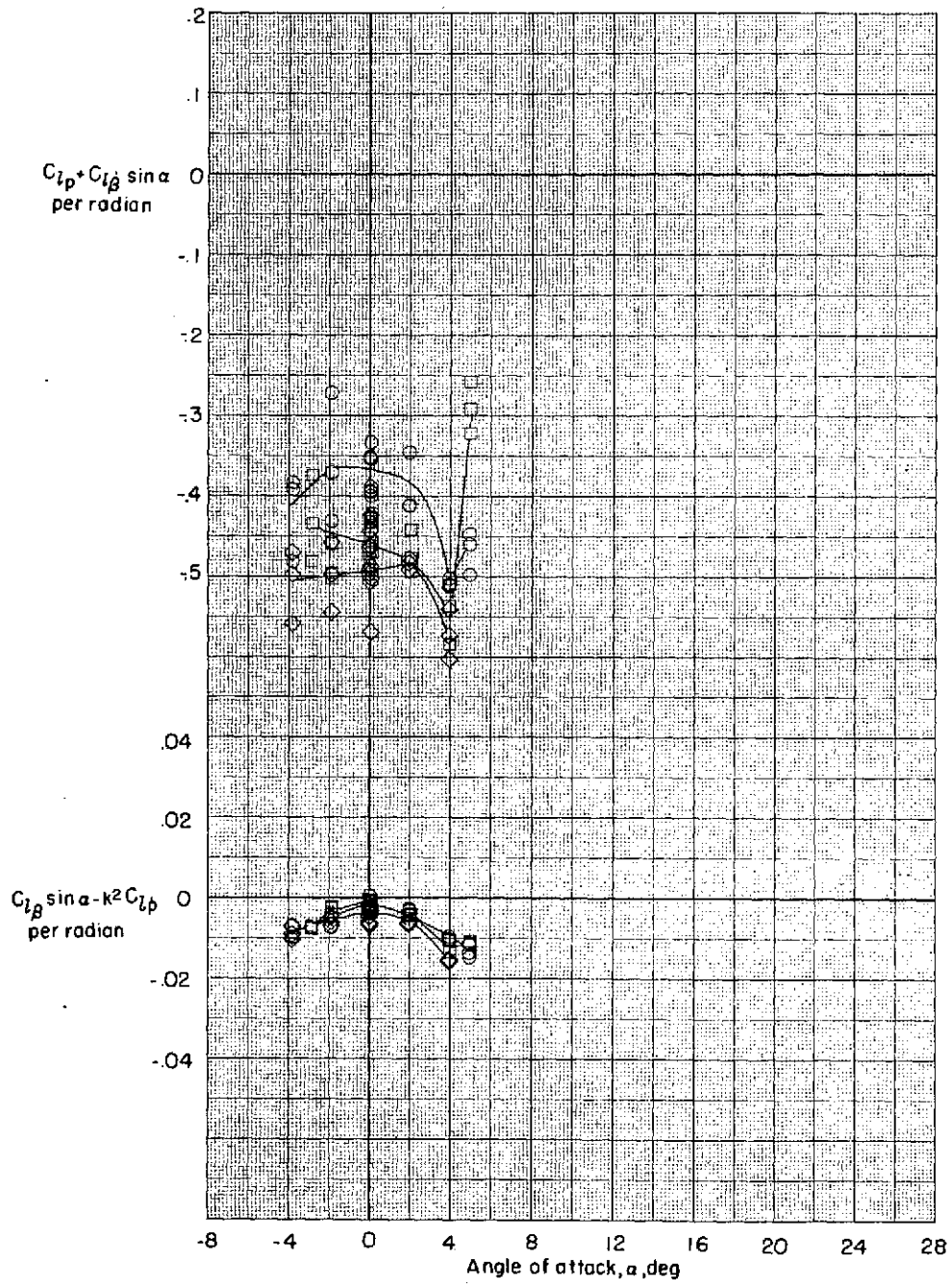
Wing	$\Lambda$	A.R.	M	k
○	10	35°	4	0.60
□	11	↓	5	↓
◇	2	↓	6	↓



(c)  $M = 0.60$ .

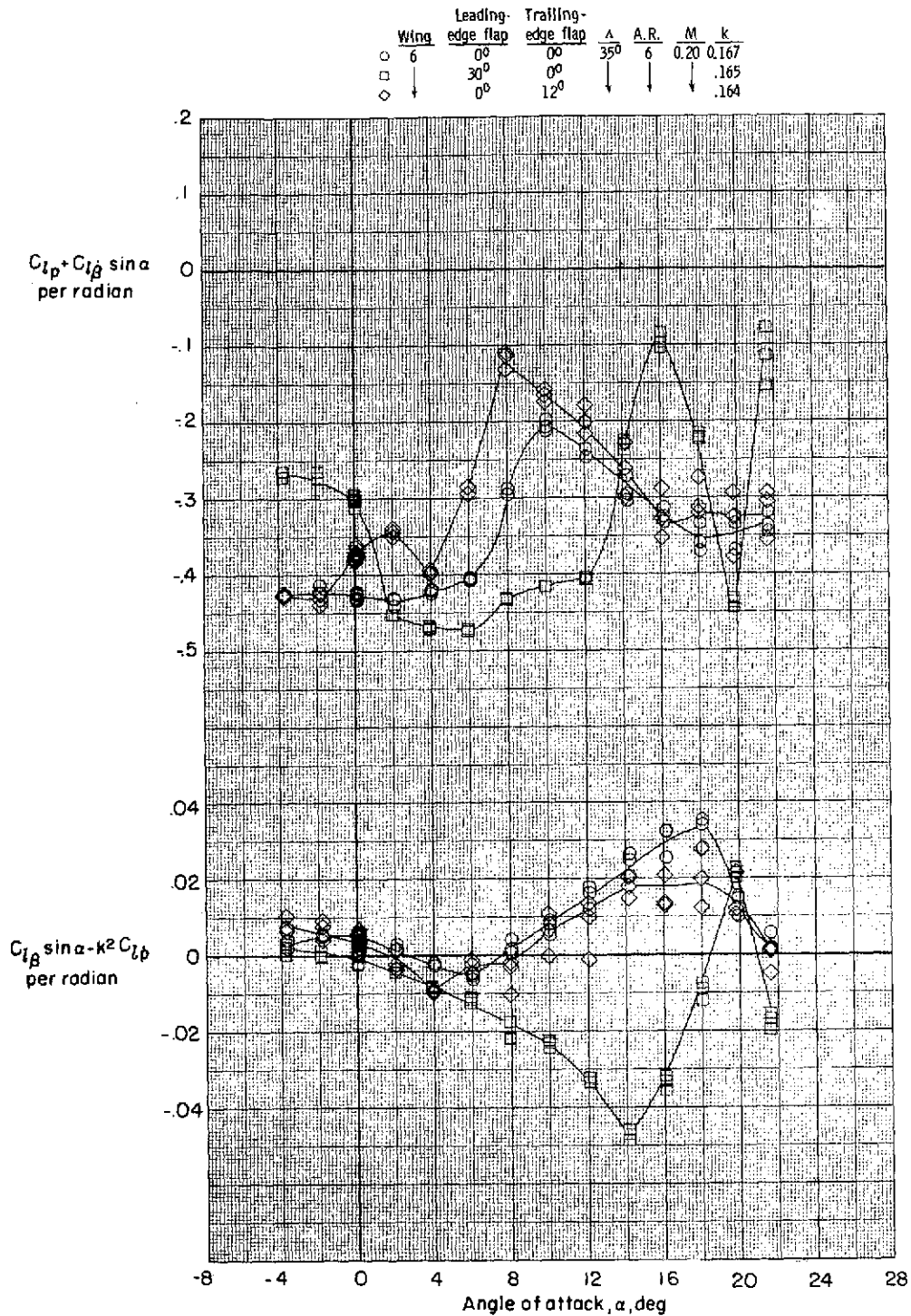
Figure 6.- Continued.

	Wing	$\Delta$	A.R.	M	k
○	10	35°	4	0.80	0.034
□	11	↓	5	↓	.039
◇	2	↓	6	↓	.042



(d)  $M = 0.80$ .

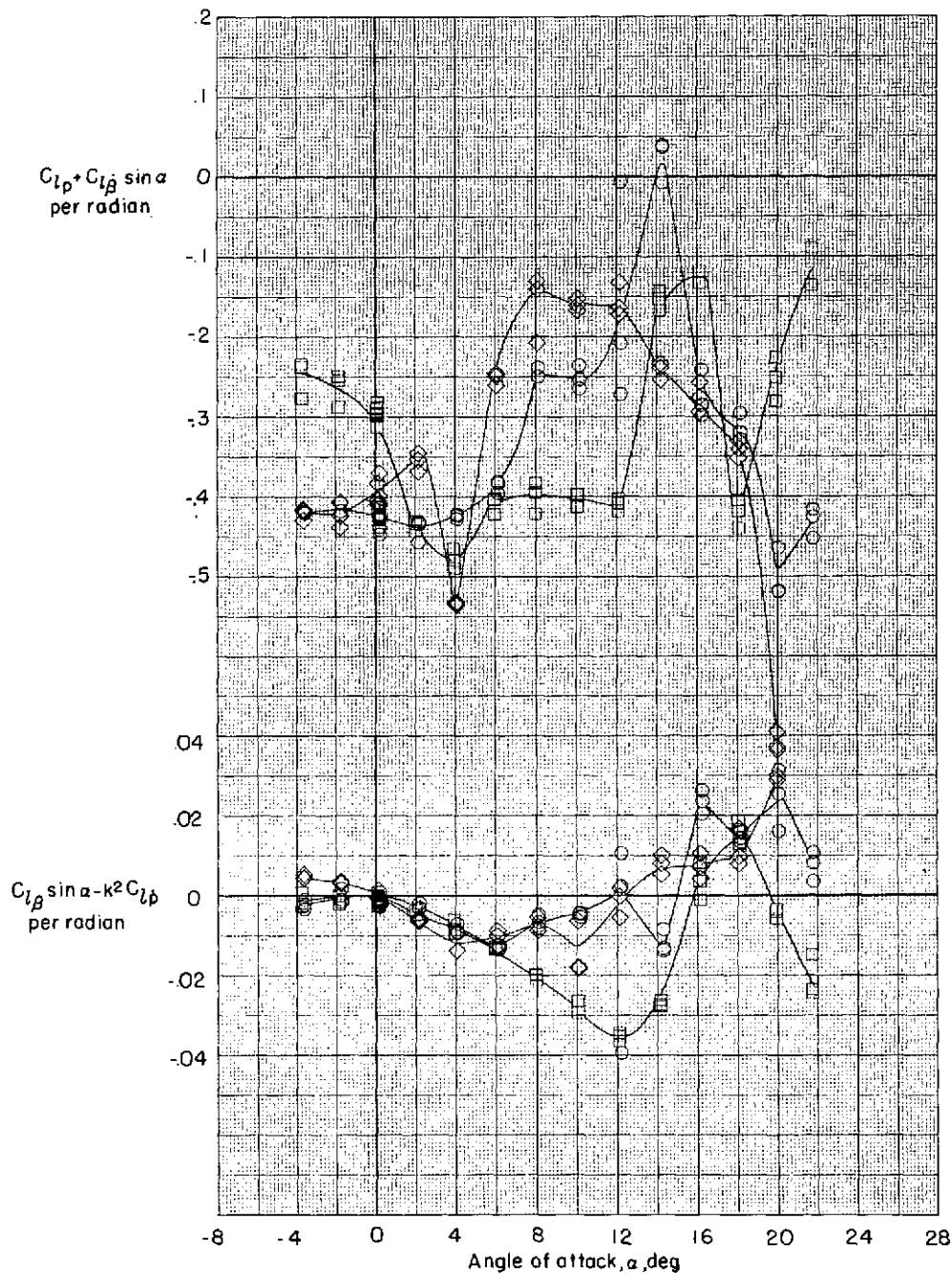
Figure 6.- Concluded.



(a)  $M = 0.20$ .

Figure 7.- Oscillatory damping in roll and rolling moment due to roll displacement characteristics of a wing with leading- and trailing-edge flap deflection.

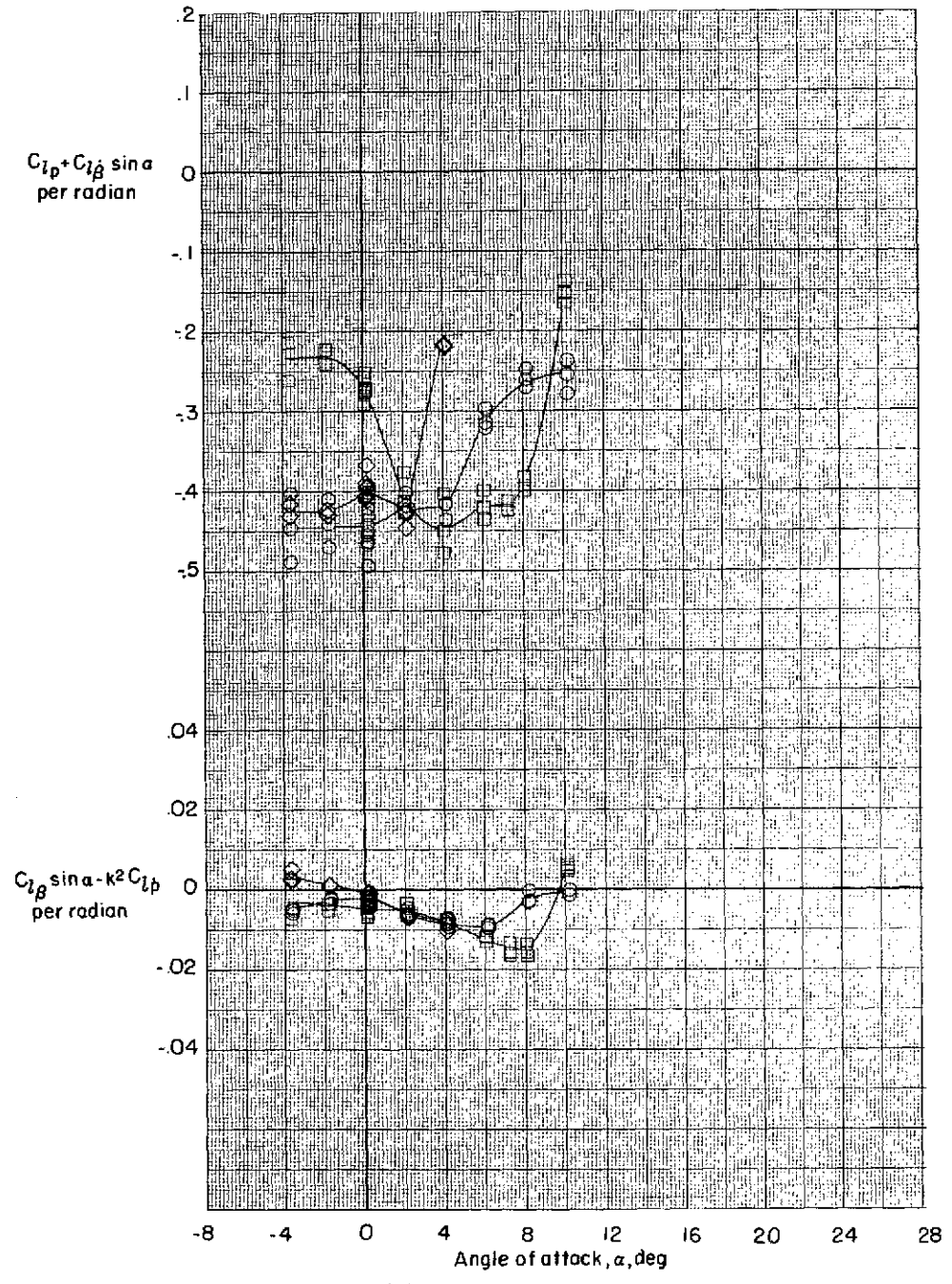
	Wing	Leading-edge flap	Trailing-edge flap	$\Lambda$	A.R.	M	k
○	6	0°	0°	35°	6	0.40	0.084
□	↓	30°	0°	↓	↓	↓	.083
◇	↓	0°	12°	↓	↓	↓	.083



(b)  $M = 0.40$ .

Figure 7. - Continued.

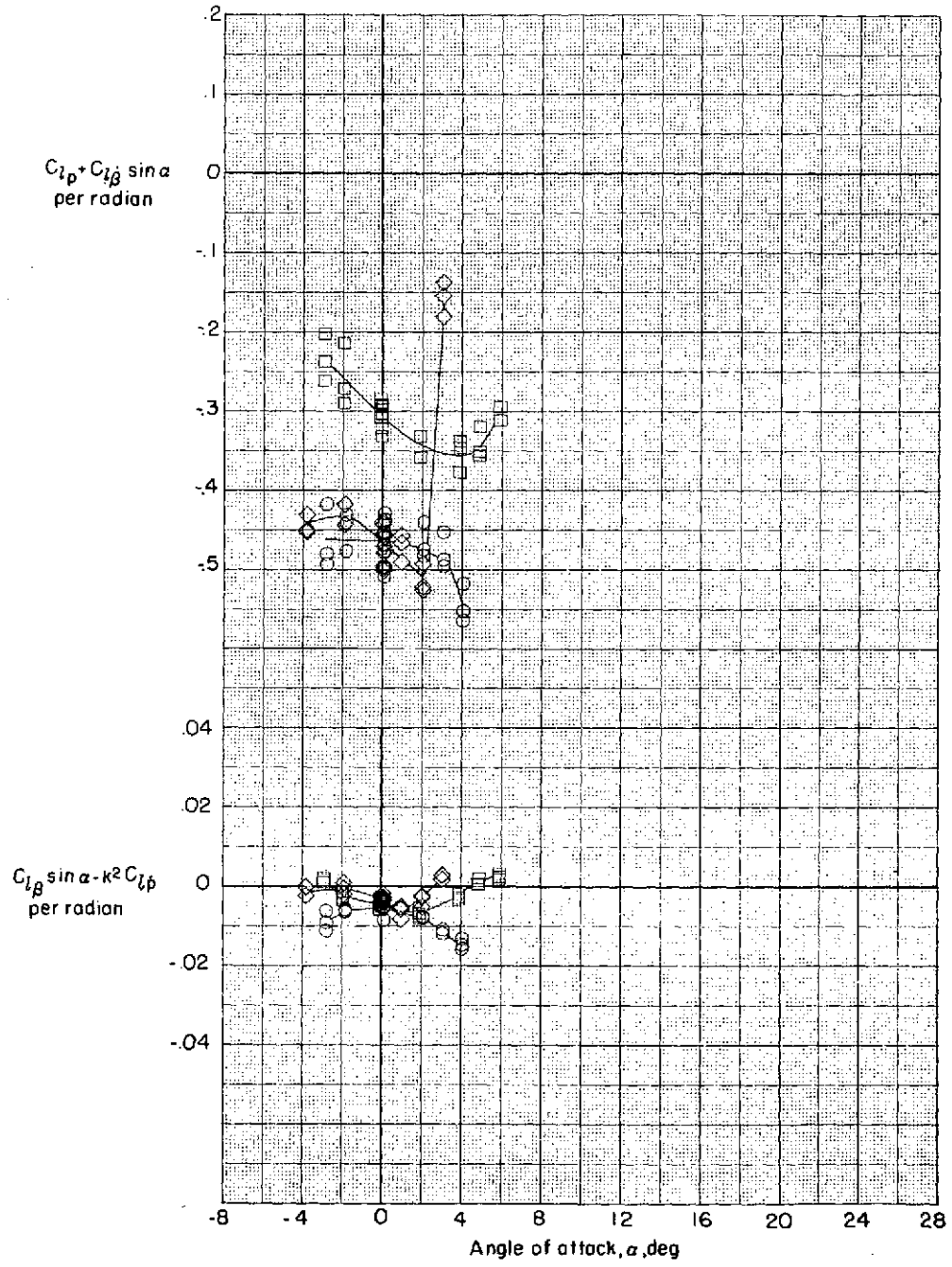
	Wing	Leading- edge flap	Trailing- edge flap	$\Lambda$	A.R.	M	k
○	6	0°	0°	35°	6	0.60	0.056
□	↓	30°	0°	↓	↓	↓	.056
◇	↓	0°	12°	↓	↓	↓	.057



(c)  $M = 0.60$ .

Figure 7.- Continued.

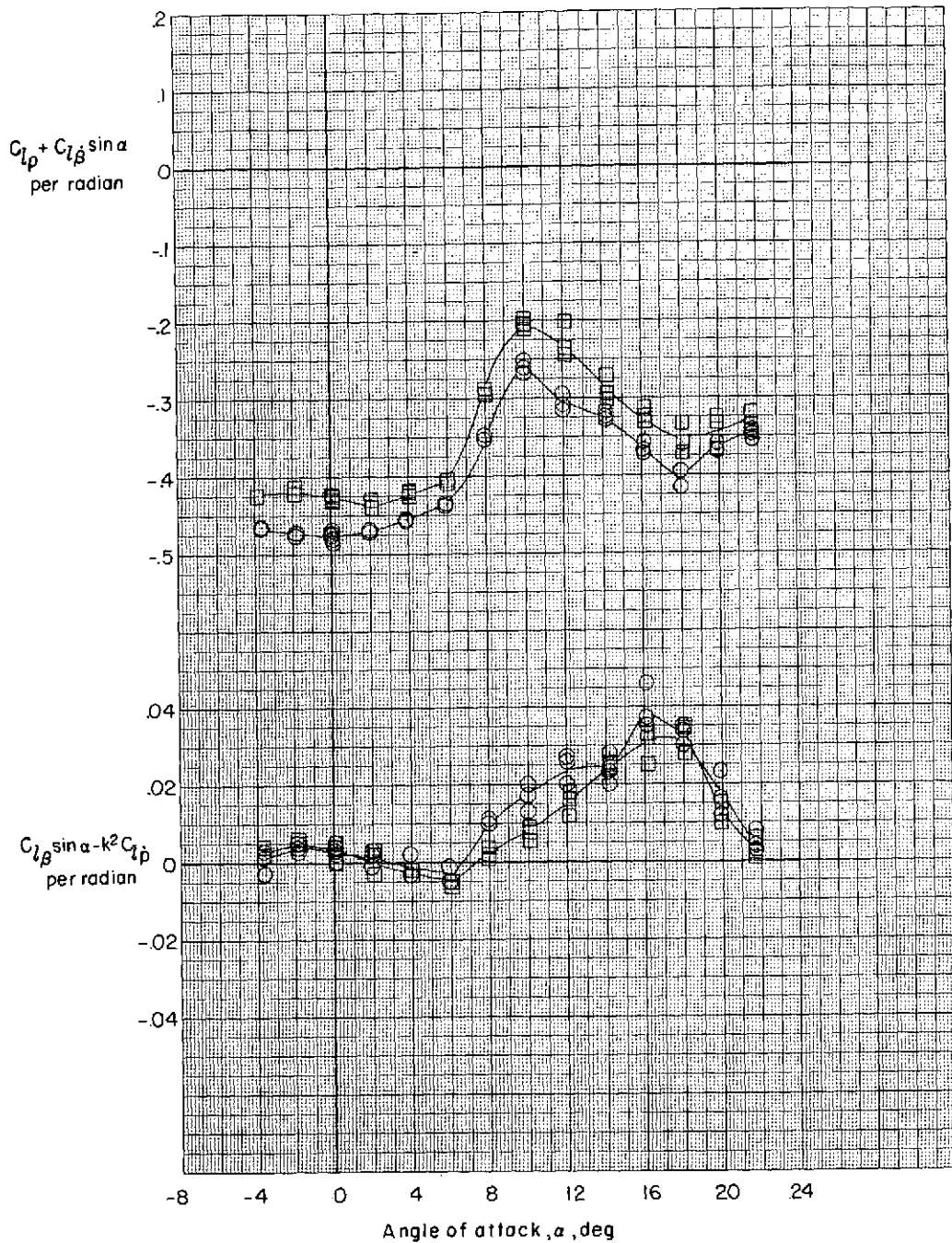
	Wing	Leading- edge flap	Trailing- edge flap	$\Lambda$	A.R.	M	k
○	6	0°	0°	35°	6	0.80	0.042
□	↓	30°	0°	↓	↓	↓	.042
◇	↓	0°	12°	↓	↓	↓	.043



(d)  $M = 0.80$ .

Figure 7.- Concluded.

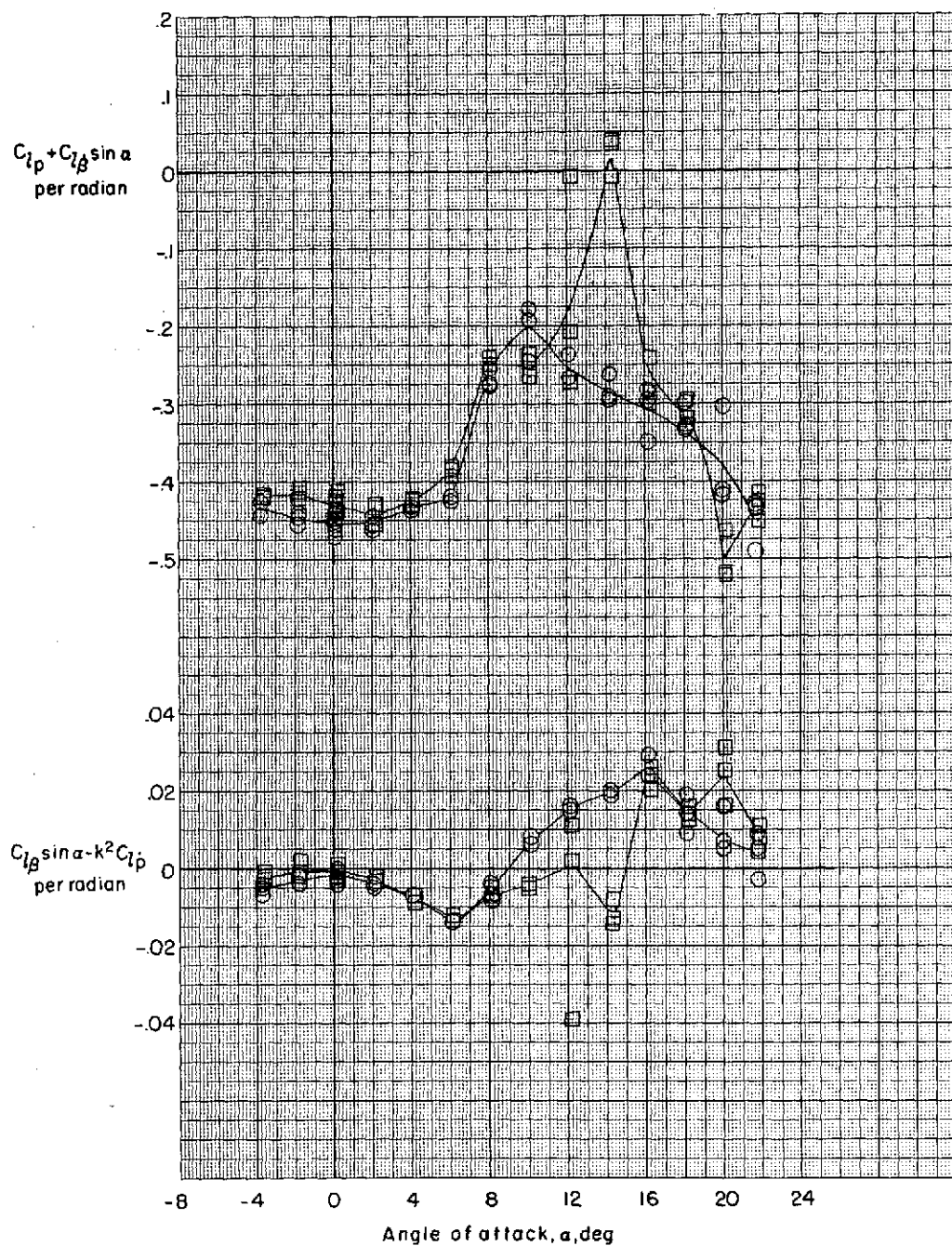
Wing	$\Lambda$	A.R.	M	Airfoil	k	
○	2	35°	6	D.20	63A008	0.208
□	6	↓	↓	↓	64A008	.167



(a)  $M = 0.20$ .

Figure 8.- Oscillatory damping in roll and rolling moment due to roll displacement characteristics of a wing with a variation in the airfoil section.

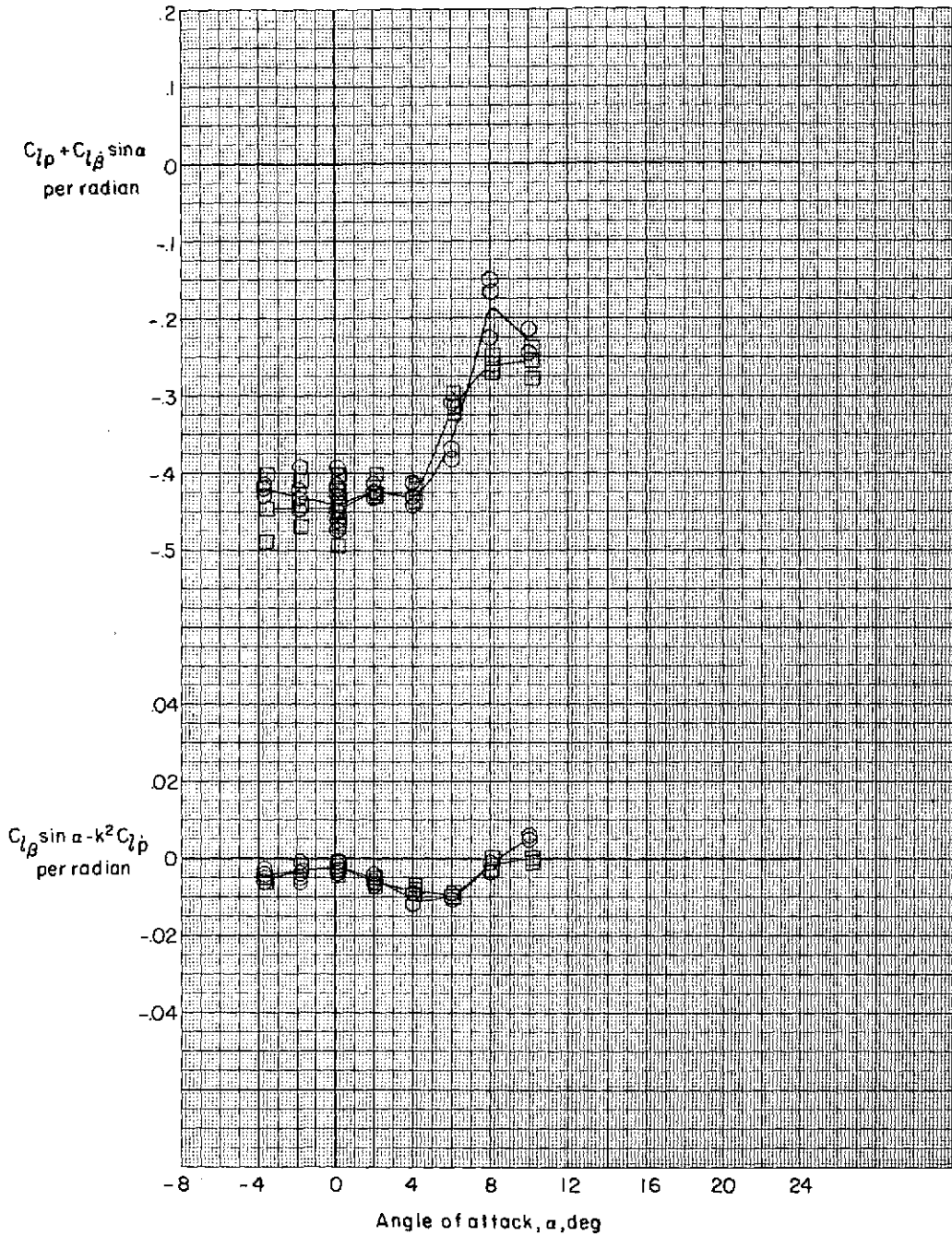
	Wing	$\Lambda$	A.R.	M	Airfoil	k
○	2	35°	6	0.40	63A008	0.104
□	6	↓	↓	↓	64A008	.084



(b)  $M = 0.40$ .

Figure 8.- Continued.

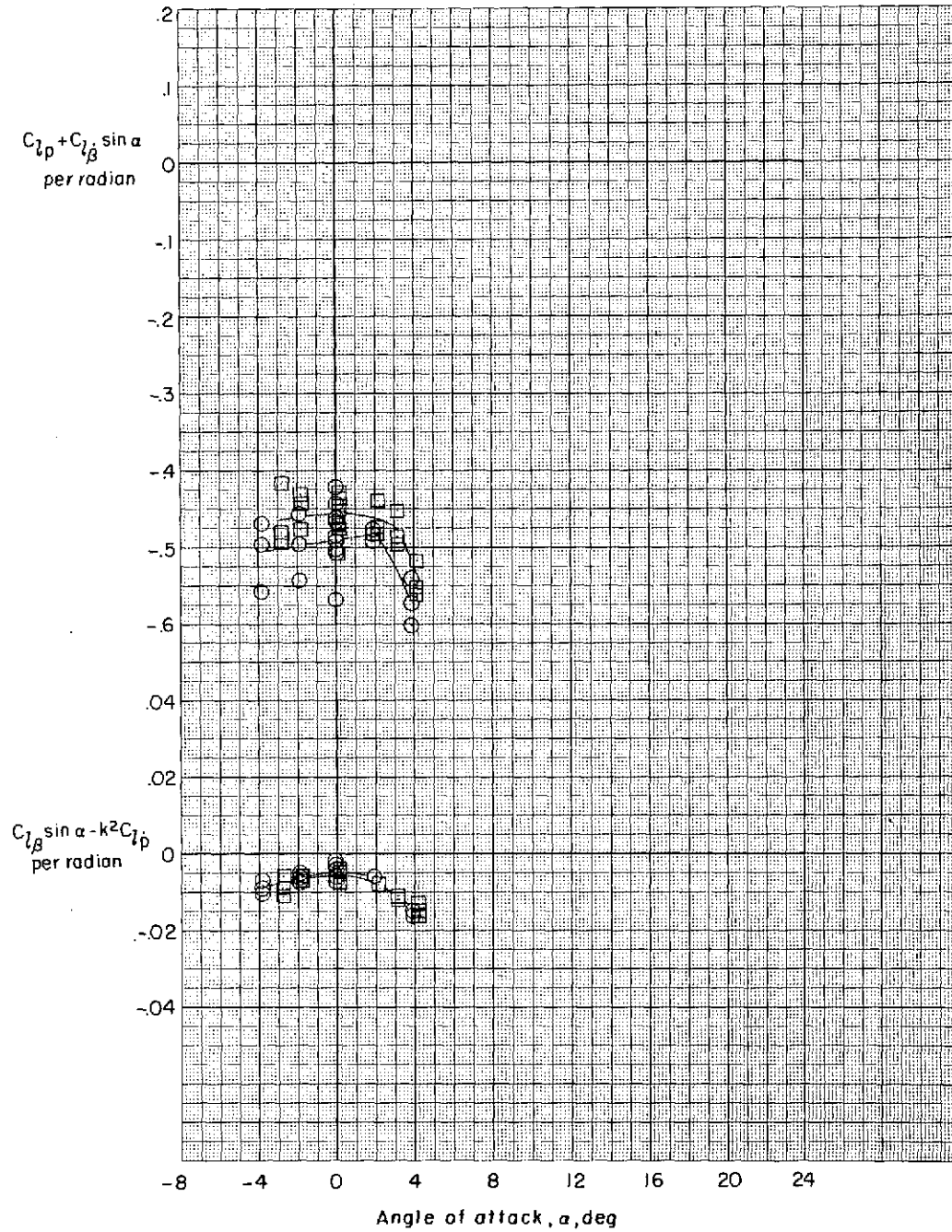
	Wing	$\Lambda$	A.R.	M	Airfoil	k
○	2	35°	6	0.60	63A008	0.055
□	6	↓	↓	↓	64A008	.056



(c)  $M = 0.60$ .

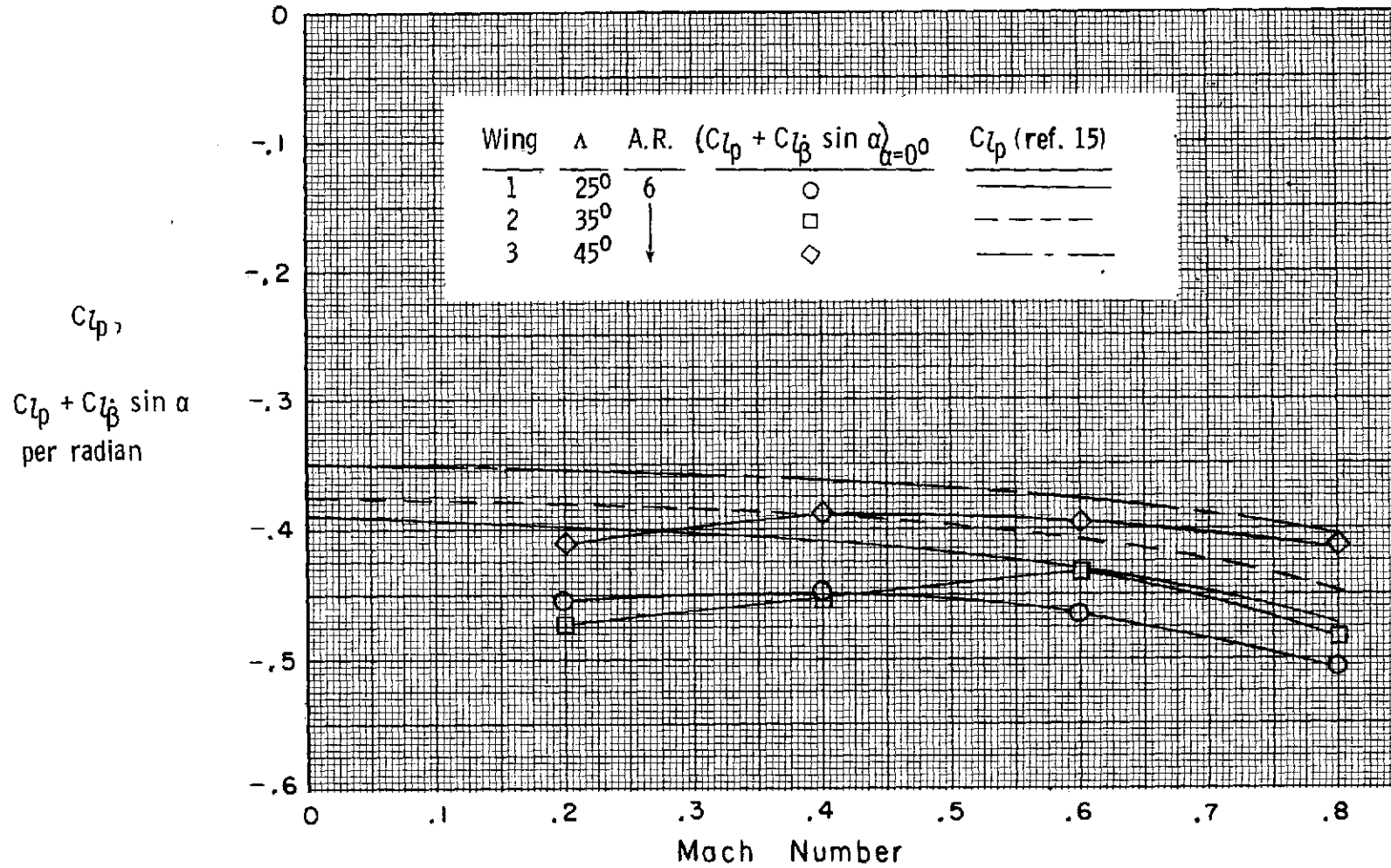
Figure 8. - Continued.

	Wing	$\Delta$	A.R.	M	Airfoil	k
○	2	35°	6	0.80	63A008	0.042
□	6	↓	↓	↓	64A008	↓



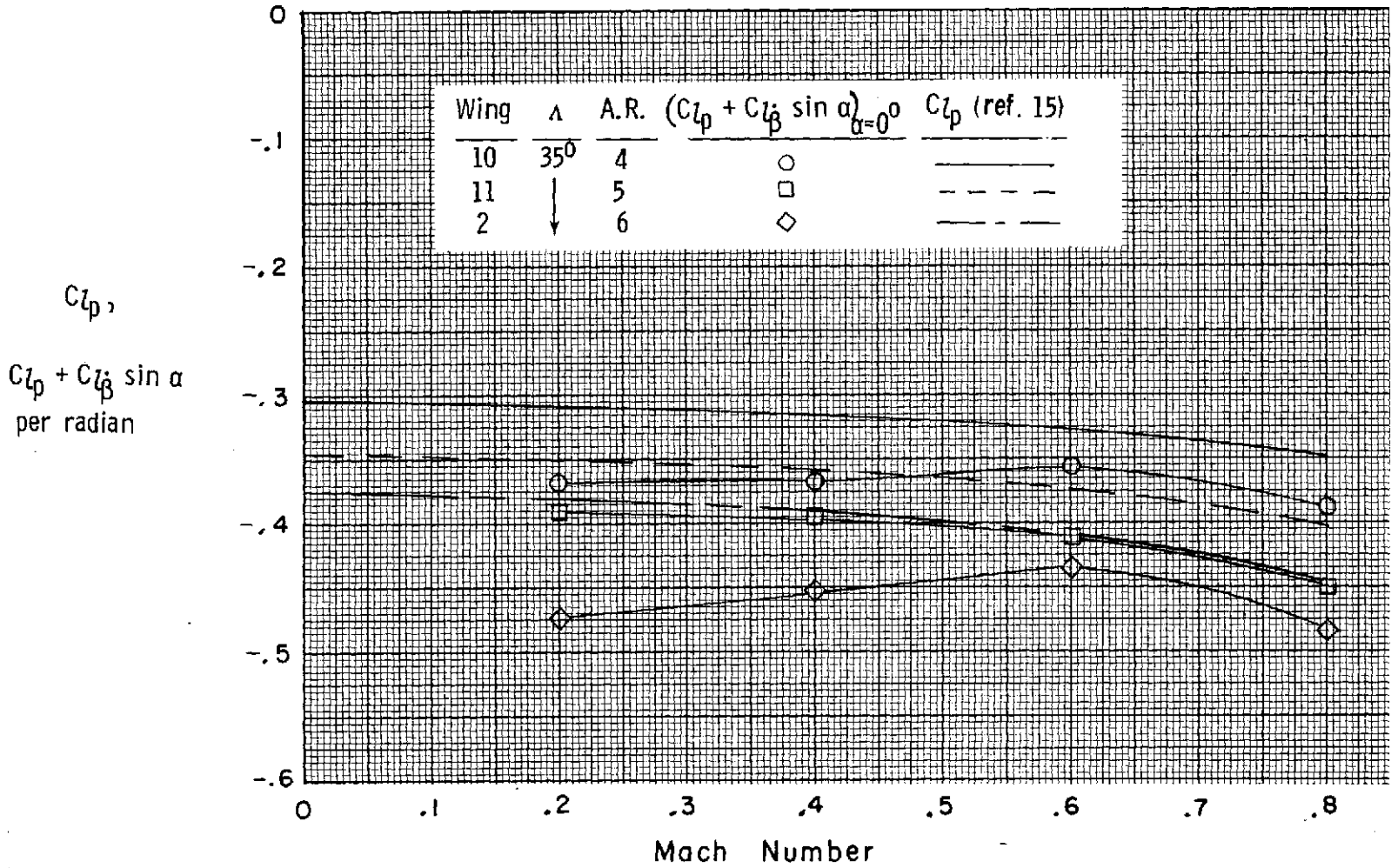
(d)  $M = 0.80$ .

Figure 8.- Concluded.



(a) Wing-sweep series.

Figure 9.- Comparison of experimental and theoretical damping in roll for  $\alpha = 0^\circ$ .



(b) Aspect-ratio series.

Figure 9.- Concluded.